Tesi di Dottorato

Noise-Induced Effects on electron transport in Silicon Structures

Effetti Indotti dal Rumore sul trasporto elettronico in Strutture di Silicio

Tutor:
Prof.ssa Dominique Persano Adorno

Dottoranda:
Dott. Ing. Maria Antonietta Lodato

Coordinatore:
Prof. Bernardo Spagnolo

SSD: Fis03

Universita` degli Studi di Palermo - Dipartimento di Fisica e Chimica

---

Corso di DOTTORATO DI RICERCA INTERNAZIONALE in FISICA APPLICATA
XXV CICLO - 2014

Contents

Commonly Used Abbreviations

Brillouin Zone: BZ

Density Of States: DOS

Very-Large-Scale Integration: VLSI

Stochastic Resonance: SR

Noise Enhanced Stability: NES

Resonant Activation: RA

Integrated Spectral Density: ISD

Monte Carlo: MC

MetalOxide Semiconductor: MOS

Density Of States: DOS

Molecular Beam Epitaxy: MBE

Metalorganic Vapour Phase Epitaxy: MOCVD

Quasi-Two-Dimensional Electron Gas: 2DEG

Metal Oxide Semiconductor Field Effect Transistor**:** MOSFET

Bulk Semiconductor: 3DEG

Boltzmann Transport Equation: BTE

Single-particle Monte Carlo: SMC

Ensemble Monte Carlo: EMC

Ornstein-Uhlenbeck: OU

Dichotomous Noise: DM

Elliot-Yafet: EY

Dyakonov-Perel: DP

Acoustic phonon: AC

Optical phonon: OP

Introduction

The study of charge transport in semiconductors is of fundamental importance, both from the point of view of basic physics, and for its application to electronic devices. On the one hand, the analysis of transport phenomena throws light on electronic interactions in crystals, band structure, lifetimes, impact ionization, etc. On the other hand, the applied aspect of the problem is even more important, since modern microelectronics, whose influence in all human activities seems to be ceaselessly growing, heavily depends on a sophisticated knowledge of many aspects of charge transport in semiconductors [1]. Starting in the early 1950s, soon after the invention of transistors, it was recognized that electric field strengths so high as to be outside of the linear-response region where Ohm's law holds were encountered in semiconductors [2]. The field of nonlinear transport (the hot-electron problem) entered a period of rapid development, and increasing numbers of researchers devoted their efforts to improving scientific knowledge on this subject. Furthermore, in the process of studying these high-field problems, new phenomena were discovered [for example, the Gunn effect (1963)] and, based on these discoveries, new devices were designed (such as transit-time devices) which, in turn, required new and deeper investigation. Thus one of the most interesting cases of positive feedback between science and technology in this century emerged. The subsequent tendency towards the miniaturization of devices, which has led to modern very-large-scale integration (VLSI) technology, has further enhanced the importance of high-field transport, since reducing the dimensions of devices has led to high-field strengths well outside the Ohmic response region for any reasonable voltage signal.

Charge transport is in general a tough problem, from both the mathematical and physical points of view. In fact, the integro-differential equation (the Boltzmann equation) that describes the problem does not offer simple (or even

complicated) analytical solutions except in a very small number of cases, and these cases are not usually applicable to real systems. Furthermore, since transport quantities are derived from the averages over many physical processes, whose relative importance is not known a priori, the formulation of reliable microscopic models for the physical system under investigation is difficult. When one moves from linear to nonlinear response conditions, the difficulties become even greater: the analytical solution of the Boltznann transport equation without linearization with respect to the external force is a formidable mathematical problem, which has resisted many attacks in the last few decades. In order to get any results, it is necessary to perform such drastic approximations that it is no longer clear whether the features of interest in the results are due to the microscopic model or to mathematical approximations.

Monte Carlo is a statistical numerical method used for solving mathematical problems; as such, it was developed well before its application to transport problems, and has been applied to a number of scientific fields [3]. In the case of charge transport, however, the statistical numerical approach to the solution of the Boltzmann equation proves to be a direct simulation of the dynamics of charge carriers inside the crystal, so that, while the solution to the equations is being worked out, any physical information required can easily be extracted. This use of the Monte Carlo makes it similar to an experimental technique; the simulated experiment can in fact be compared with an analytically formulated theory [1].

The presence of noise in semiconductor materials is generally considered a disturbance, since strong fluctuations affect performance and reliability of semiconductor-based devices. The existence of fluctuations, for example, can limit the lifetime of the information stored in a memory cell, it bothers the opening (or closure) of random logic gates and it causes the enlargement of the distribution of arrival times of signals on transmission lines. In order to fully understand the complex scenario of the nonlinear phenomena involved in the devices response, several studies have investigated hot-electron transport dynamics in bulk and semiconductor structures, by analysing the electronic noise in systems driven by external static or oscillating electric fields [4]-[16].

Recently, noise-induced complex phenomena in nonlinear systems have

increasingly been investigated, with a focus on cooperative effects between the noise and the intrinsic interactions of the system [17–37]. Previous studies have shown that, under specific conditions, an external noise can constructively interact with an intrinsically nonlinear system, characterized by the presence of intrinsic noise, giving rise to positive effects [17]-[24] such as stochastic resonance (SR) [25]-[28], resonant activation (RA) [29, 31] and noise enhanced stability (NES) [32]-[36]. In particular, the possibility of suppressing the intrinsic noise in n-type GaAs and Si bulk, driven by a static electric field, with the addition of a Gaussian correlated noise source, has been theoretically investigated [37]. Detailed studies of diffusion noise in low-doped GaAs bulk, subjected to a driving periodic electric field containing time-correlated fluctuations, have revealed the possibility of a suppression of electronic noise [34, 35]. Under specific conditions, the intrinsic noise in n-type GaAs crystals can also be reduced by adding a two-level random telegraph noise source to the driving high-frequency oscillating electric field [36]. In refs. [38, 39], a way to improve the ultra-fast magnetization dynamics of magnetic spin systems by including random fields has been discussed. In semiconductor quantum wells and wires, Glazov et al. have demonstrated that the randomness in spin-orbit coupling is inevitable and can be attributed to both the electron-electron dynamic collisions and the static fluctuations in the density of dopant ions [40, 41]. Furthermore, they pointed out the possibility of using fluctuating random Rashba spin-orbit interaction for the generation of spin currents [42]. Monte Carlo simulations have also shown that random spatial variation of the Rashba electric field along the length of a quantum wire makes the spatial spin relaxation characteristics random, nonmonotonic and chaotic [43].

The process of spin relaxation in III-V semiconductors structures has been widely investigated in recent years [44-48]. Research along this line has been motivated by the possibility of developing electronic devices that perform logic operations, communication and storage, within the same material technology. However, to use of spin polarization as an information carrier, the disadvantage that each initial non-equilibrium orientation decays over time during transport must be faced. Hence, to open the way to the implementation of spin-based devices, the features of spin relaxation at relatively high

temperatures, together with the influence of transport conditions, should first be fully understood and interpreted in experiment-related terms. Previous studies of the electron spin relaxation process in GaAs bulks, at nitrogen temperature, have shown that a random contribution added to the static electric field can affect the spin decoherence length [49, 50]. In particular, it has been found that the effect on spin depolarization length is maximum for values of the noise correlation time comparable with the characteristic time of the spin relaxation process, and that, depending on the amplitude of the applied electric field, the external fluctuations can have opposite effects [49].

Recently, electrical injection of spin polarization in n-type and p-type silicon up to room-temperature have been experimentally carried out [51-53], but theoretical research is still incomplete and a comprehensive investigation into the influence of transport conditions on the spin depolarization process in silicon structures, in a wide range of values of temperature and amplitude of external fields, is still missing.

The aims of this thesis are:

1. the investigation of the effects of the addition of an external correlated source of noise on the carrier velocity fluctuations in silicon semiconductor crystals and lower dimensional structures.

In particular:

- ✓ Characterization of bulk covalent Si semiconductors
- ✓ Research extension to 2D structures (Si inversion layer).

2. the development of a comprehensive theoretical framework concerning the influence of transport conditions on the spin depolarization process in silicon structures, by estimating both the spin lifetimes and the depolarization lengths as a function of the values of lattice temperature, electric field amplitude and doping density.

The first part of the thesis is devoted to introduce some background knowledge of the concept of noise and to investigate the effects of the addition of an external correlated source of noise on the carrier velocity fluctuations in quasi-two-dimensional silicon semiconductor structures, operating at different temperatures and under different static conditions. In our modelling of the quasi-two-dimensional electron gas, the potential profile, perpendicular to the

MOS structure, is assumed to follow the triangular potential approximation. The carrier intrinsic noise is obtained by computing the velocity fluctuation correlation function and its spectral density [54-55]. The modifications caused by the addition of an external source of correlated noise are investigated by analysing the noise integrated spectral density (ISD), which coincides with the variance of the electron velocity fluctuations, as a function of the characteristic parameters of the added fluctuations. In order to elucidate the effects of the correlated noise source on the intrinsic noise properties, we have performed 100 different realizations and evaluated both average values and error bars for the calculated integrated spectral densities.

In the second part of the thesis we study the hot-carrier noise in low-doped n-type Si crystals operating under a periodic electric field with different frequencies and the noise-induced effects on electron transport dynamics. In the latter case, the system is driven by a high-frequency periodic electric field, in the presence of two different kinds of external fluctuations: a Gaussian correlated or a Random Telegraph noise source. In order to elucidate the effects of the correlated noise source on the intrinsic noise properties, we have performed 200 different realizations for the calculated integrated spectral densities. The results are discussed and compared with those obtained in the absence of the exsternal source of noise.

The last investigation presented in this thesis show the results of the spin dynamics in n-type Si crystals obtained by using a semiclassical Monte Carlo (MC) approach to simulate both the electron transport and the spin dynamics. Spin relaxation is taken into account through the Elliot-Yafet mechanism [56, 57], which is dominant in group IV materials. Despite our MC code does not take into account the scattering of electrons with g-phonons, the interactions with the impurities and uses approximated relations for the spin-flip rates, we found a good agreement with the analytical theories in absence of applied electric fields.

Our validated MC algorithm provides the experimental researchers with an estimate of spin lifetimes of drifting electrons in n-type Si crystals, at different temperatures and under different electron transport conditions.

Chapter 1

Basic Semiconductor Physics

In the first part of this chapter, we present a short summary of the main physical properties of semiconductors and we give basic information on the carrier dynamics in bulk semiconductors [58]-[61]. In the second part, we do the same for the Monte Carlo (MC) approach, used to study the transport properties in semiconductor structures. This method is widely used for modelling charge carrier transport in semiconductor structures and modern devices. Due to its flexibility, this approach can easily take into account many scattering mechanisms, specific device design, material properties and boundary conditions in the simulation (for more details see Ref. [62]-[64].

1.1 Structure and Energy Band of Silicon [59]

Commonly, Silicon (Si) crystallizes in a diamond structure on a face-centered cubic (f.c.c.) lattice, with a lattice constant of a_o=5.43 Å. The basis of the diamond structure consists of two atoms with coordinates (0,0,0) and a_o/4 (1,1,1) as shoun in Fig.1.1.

The Brillouin zone (BZ), i.e. the primitive cell in the reciprocal-space lattice, which is a body-centered cubic (b.c.c.) lattice, together with important reference points and directions within it, is shown in Fig. 1.2.

Electrons in a semiconductor crystal move in a periodic crystal potential, which consists of the potential due to the atomic nuclei and of that due to the

electrons themselves. Therefore, when we study the electron transport in a crystal, we have to deal with an extremely complicated many-body problem.

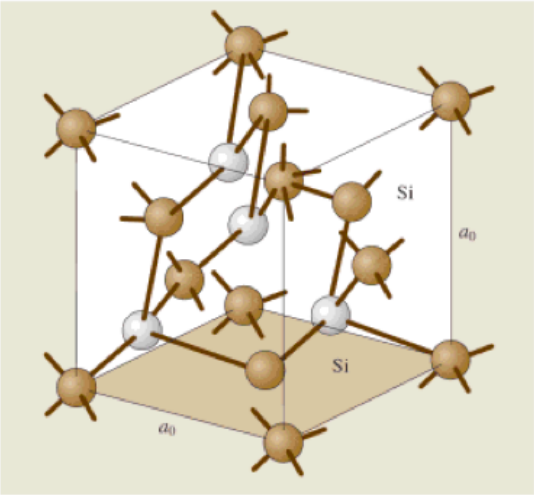

Figure 1.1 Diamond crystal structure of Si [59]

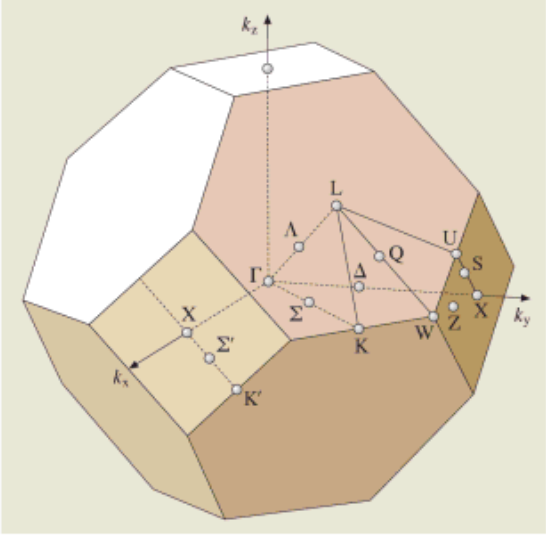

Figure.1.2 Brillouin zone of the f.c.c. lattice [59]

However, if we pay attention to the motion of an electron in the crystal and assume that the effect of the atomic nuclei and the remaining electrons on the selected electron can be approximated by a given potential V(r), the many-body problem can be reduces to the problem of a single electron V(r) is periodic with the same periodicity of the lattice. This property is mathematically expressed as

$$V(\boldsymbol{r} + l\boldsymbol{a} + m\boldsymbol{b} + n\boldsymbol{c}) = V(\boldsymbol{r}) \tag{1.1}$$

where $\boldsymbol{a}$, $\boldsymbol{b}$, and $\boldsymbol{c}$ are the primitive basis vectors, and l, m, and n are integers. To determine the electronic states for a periodic potential V(**r**), we have to solve the Schrodinger equation

$$\left[-\frac{\hbar^2}{2m_0}\nabla^2 + V(\boldsymbol{r})\right]\psi(\boldsymbol{r}) = E\psi(\boldsymbol{r}) \tag{1.2}$$

where $\psi(\boldsymbol{r})$ is the eigenfunction to be determined, E is the energy eigenvalue, m_0 is the electron mass in free space, $\hbar$ is Planck's constant divided by 2π, and $\nabla^2$is the Laplacian operator. According to the Bloch theorem, the solutions for a perfectly periodic potential have the following form:

$$\psi(\boldsymbol{r}) = e^{i\boldsymbol{k}\cdot\boldsymbol{r}}u_{s\boldsymbol{k}}(\boldsymbol{r}) \tag{1.3}$$

where $\boldsymbol{k}$ is the wave vector that runs over reciprocal space, s is a band index and $u_{s\boldsymbol{k}}(\boldsymbol{r})$ is the periodic function of the direct lattice (Bloch amplitude). Both $u_{s\boldsymbol{k}}(\boldsymbol{r})$ and the corresponding energy-band spectrum $E_s(\boldsymbol{k})$ are periodic in $\boldsymbol{k}$, which allows one to restrict consideration within the BZ.

The bands are arranged so that there are energy regions for which no states given by (1.3) exist. Such forbidden regions are called energy gaps or band gaps and result from the interaction of valence electrons with the ion cores of crystals.

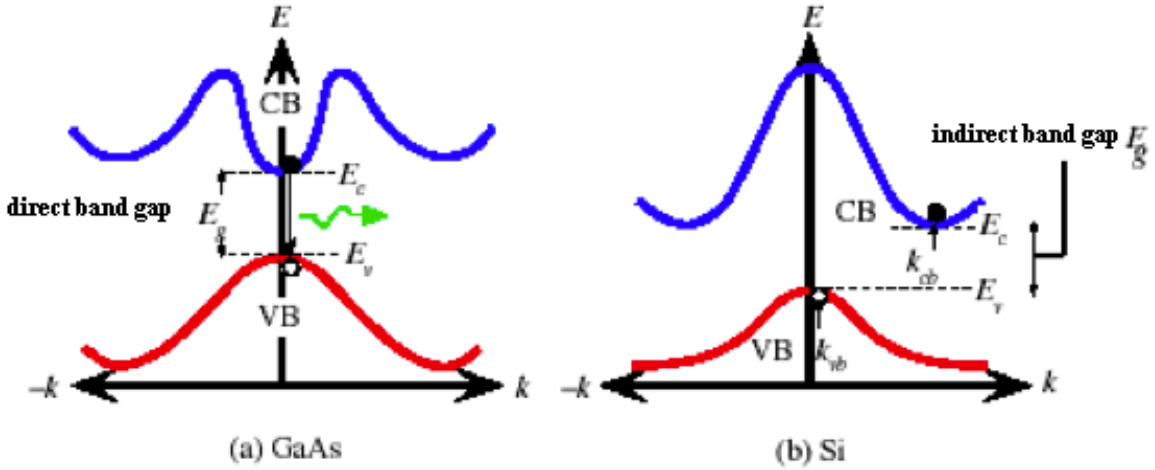

Figure 1.3: Band gap (a) in GaAs and (b) in Si

In semiconductor science the term *band gap* is accepted for the energy distance between the maximum of $E_s(\boldsymbol{k})$ for the highest filled (valence) band and the minimum of $E_s(\boldsymbol{k})$ for the lowest empty (conduction) band (denoted by E_g) (Fig. 1.3). The band gap is called *direct* if the aforementioned maximum and minimum occur at the same point of the BZ, e.g. Γ, , and *indirect* if they occur at different points of the BZ, e.g. Γ and X.

Si is an indirect-band-gap semiconductor with $E_g = 1.17\,eV$ at 4.2K. The calculated energy-band structure, that is the curves of $E_v(\boldsymbol{k})$ for selected directions in the BZ, is shown in Fig. 1.4a. The conduction-band minimum lies at six equivalent points Δ on the Γ-X lines (Fig. 1.4a).

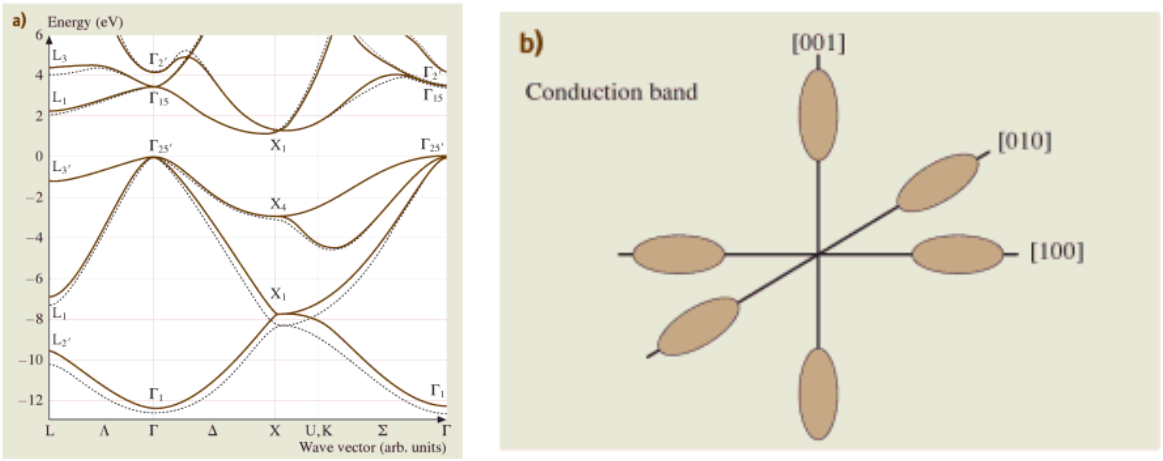

Figure. 1.4: Electronic band structure of Si: (a) Energy dispersion curves near the fundamental gap. (b) The constant-energy of the conduction band [59]

At the bottom of eah valley the band spectrum is quadratic in $\boldsymbol{k}$, e.g. for the valley ⟨1 0 0⟩

$$E_c(\boldsymbol{k}) = E_{c0} + \frac{\hbar^2(k_x - k_0)^2}{2m_l} + \frac{\hbar^2\left(k_y^2 + k_z^2\right)^2}{2m_t} \tag{1.4}$$

where $k_0 \approx 1.72\pi/a_0$, m_l and m_t are the longitudinal and transverse effective masses. The spectra for the other five valleys are obtained from (1.4) by 90° rotations and inversions $k_0 \to -k_0$. Though the constant-energy surface for (1.4) is an ellipsoid (Fig. 1.4b), the density of states (DOS) proves to be the same as for an isotropic parabolic spectrum with an effective mass

$$m_{de} = 6^{2/3} m_l^{1/3} m_t^{2/3} \tag{1.5}$$

which is called the DOS *effective mass*.

Equation 1.4 holds at $E_c - E_{c0} < 0.15eV$, but at larger energies the ellipsoids strongly warp , especially near the X point; the change of the spectrum with energy is mostly due to the increasing m_t, while m_l weakly increases [62].

The valence-band maximum is at the Γ point ($\boldsymbol{k}$=0) where the Bloch-wave state $u_{n0}(\boldsymbol{r})$ has the full symmetry of an atomic p-orbital, being six-fold degenerate in the nonrelativistic limit.

1.2 Electron Dynamics [65]

As discussed in the previous section, electrons in a crystal behave just like electrons in free space, except for a change in their mass. This fact suggests that the motion of electrons in a crystal may be described by the classical equations of motion. This idea is acceptable if the potential energy felt by electrons varies slowly compared to the crystal potential, and quantum mechanical effects such as reflection and tunnelling can therefore be ignored. The classical motion of an electron is described by the equations of motion based on the total energy (or Hamiltonian), $H = E_k + U$, where E_k is the kinetic energy and U is the potential energy. The motion of an electron in a conduction band can also be described if we properly choose the Hamiltonian as [65]

$$H = E_{\boldsymbol{k}} + E_c(\boldsymbol{r}) \tag{1.6}$$

where $E_{\boldsymbol{k}}$ represents the kinetic energy in terms of the crystal momentum and the effective mass, and $E_c(\boldsymbol{r})$ is the conduction band minimum given by

$$E_c(\boldsymbol{r}) = \text{constant} - \chi(\boldsymbol{r}) - eV(\boldsymbol{r}) \tag{1.7}$$

where $\chi(\mathbf{r})$ is the electron affinity, e is the magnitude of the electronic charge, $V(\mathbf{r})$ is the electrostatic potential, and the *constant* is related to the reference of electron energy. If the material is compositionally uniform, $\chi(\mathbf{r})$ is constant and can be eliminated from (1.7).

Figure 1.5 shows the case of an electron moving in a slowly varying potential without scattering. In the case of hole motion in the valence band, $E_c(r)$ in (1.6) has to be replaced by the energy of the valence band maxima, $E_v(r)$.
The equations of motion can easily be constructed by using an analogy with Hamilton's equations of motion.

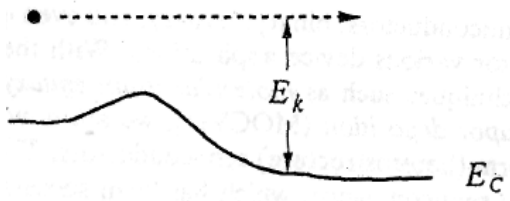

Figure 1.5: Motion of an electron moving in a slowly varying potential E_c without scattering E_k is the kinetic energy of the electron [65].

Thus, we have

$$\frac{d\mathbf{k}}{dt} = -\frac{1}{\hbar}\nabla H \tag{1.8a}$$

$$\frac{d\mathbf{r}}{dt} = \frac{1}{\hbar}\nabla_k H \tag{1.8b}$$

where ∇ and ∇_k are del operators with respect to position vector $\mathbf{r}$ and wave vector $\mathbf{k}$, respectively. For spherical and ellipsoidal bands, equation (1.8b) gives the following simple results for the group velocity:

$$\boldsymbol{v} = \frac{\hbar \boldsymbol{k}}{m^*} \tag{1.9}$$

and

$$\boldsymbol{v} = \frac{\hbar \boldsymbol{k_l}}{m_l^*} + \frac{\hbar \boldsymbol{k_t}}{m_t^*} \tag{1.10}$$

which have similar forms of free electron momentum divided by mass. For the non-parabolic band, the group velocity calculated by (1.8b) is

$$\boldsymbol{v} = \frac{\hbar \boldsymbol{k}}{m^*}\frac{1}{\sqrt{1+4\alpha\gamma(k)}} \tag{1.11}$$

1.2.1 Carrier Confinement in Heterostructures

With the use of modern epitaxial growth techniques (MBE, MOCVD, etc.), the alloy composition can be varied on an atomic scale, and very sophisticated layer structures consisting of several barriers and wells can be constructed. Electrons in the quantum well are termed quasi-two-dimensional electron gas (2DEG) because of the confined electron motion in the well. The consideration of 2DEG is very important, since this quantum confinement is observed in modern heterostructure devices as well as in the conventional silicon MOSFETs [66].

We assume that the electron motion is confined in the *z*-direction but it is free in the *x*-*y* plane. This electron motion can be analyzed by the three-dimensional Schrödinger equation:

$$-\frac{\hbar^2}{2m_0}\nabla^2\psi(\boldsymbol{r}) + E_c(\boldsymbol{r})\psi(\boldsymbol{r}) = E\psi(\boldsymbol{r}) \tag{1.12}$$

The first step to solving (1.12) for 2DEG is to apply the separation of variables which reduce the problem lower dimensions. Because carriers are free to move in the *x*-*y* plane, it is very natural to use plane wave solutions in the *x*-*y* direction; thus,

$$\Psi(\boldsymbol{r}) = C\psi(z)\cdot e^{ik_x x}e^{ik_y y} \tag{1.13}$$

where C is the normalization constant. Substituting (1.13) into (1.12), we find an equation for $\psi(z)$:

$$-\frac{\hbar^2}{2m_0}\frac{\partial^2\psi(z)}{\partial z^2} + E_c(z)\psi(z) = E_n\psi(z) \tag{1.14}$$

where

$$E_n = E - \mathrm{E}_{\|} = E - \frac{\hbar^2}{2m^*}\left(k_x^2 + k_y^2\right) \tag{1.15}$$

is the energy associated with confinement in the z-direction and $E_{\|}$ is the kinetic energy associated with the motion parallel to the x-y plane. To find $\psi(z)$ and E_n by solving the wave equation, the potential energy $E_c(z)$ has to be specified.

If the quantum well is square and infinitely deep, then $\psi(z)$ is given by the infinite number of solutions:

$$\psi(z) = \sqrt{\frac{2}{W}} sink_z z \tag{1.16}$$

where $\sqrt{2/W}$ is the normalization constant and k_z is restricted to discrete values given by

$$k_z = \frac{n\pi}{W} \tag{1.17}$$

where n is a positive integer and W is the width of the well. The corresponding energy due to confinement in the z-direction is also restricted to

$$E_n = \frac{\hbar^2 k_z^2}{2m^*} = \frac{\hbar^2}{2m^*}\left(\frac{n\pi}{W}\right)^2 \tag{1.18}$$

According to (1.18), $E = E_n + E_{\|}$; therefore, the electron energy can increase in each subband. E_n thus denotes the bottom energy of each subband. E_n increases with the decrease of the width of the well.

The density of states for the n^{th} subband (per given spin and per unit energy range) is independent of E and is given by

$$N_n(E) = \frac{m^*}{2\pi\hbar^2 W} \tag{1.19}$$

If W is eliminated from (1.19) by substituting (1.18), we then have an alternative form for the density of states for the nth subband:

$$N_n(E) = \frac{(2m^*)^{3/2}}{4\pi^2\hbar^3}\left(\sqrt{E_n} - \sqrt{E_{n-1}}\right) \qquad \text{for } E > E_n \tag{1.20}$$

where E_1 is the energy level of the ground-state subband and E_0 is defined as the bottom energy of the well; thus, $E_0 = 0$. Equation (1.20) can also be applied for a quantum well with an arbitrary shape if the subband energies are known. Equation (1.20) clearly shows how the density of states for 2DEG is related to that of bulk electrons (3DEG):

$$N(E_k) = \frac{(2m^*)^{3/2}}{4\pi^2\hbar^3}\sqrt{E_k} \tag{1.21}$$

The density of states for 2DEG and 3DEG are shown in Fig. 1.6, which shows that the total density of states for 2DEG coincides with that for 3DEG when $E = E_n$.

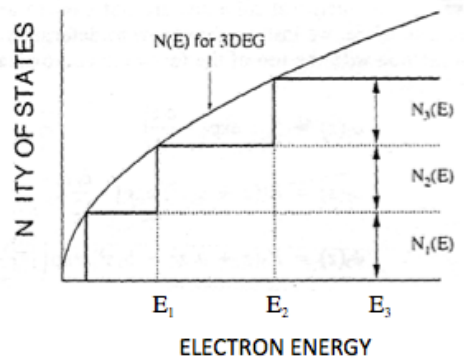

Figure 1.6 Density of states for 2DEG as a function of electron energy. The thick solid line shows the total density of states of 2DEG, and the thin solid curve shows that of 3DEG, $N_i(E)$ is the density of states of the i^{th} subband and E_i is the subband energy level [65].

In many practical cases, the Schrödinger equation (1.14) cannot be solved analytically. Approximate methods, such as a variational method and the Wentzel-Kramers-Brillourin (WKB) method, are used to evaluate 2DEG states. Fig. 1.7 shows the case of the presence of a constant electric field over an infinite potential barrier, which elestically reflects electrons. This is known as triangular potential well

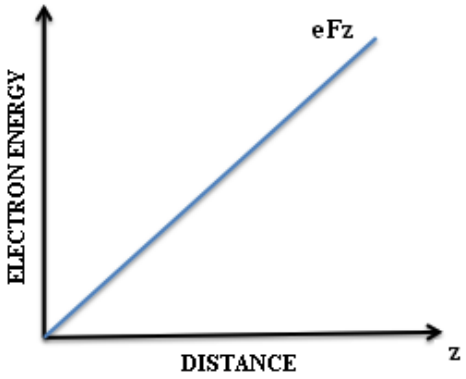

Figure 1.7: Triangleular potential well. F (the slope of the line) shows the magnitude of the electric field.

1.3 Boltzmann's Transport Equation [67, 74]

In the description of an electronic device, like a transistor or a diode, the usual approach is to consider the electronic current as a fluid, but in the reality the current consists of single particles free to move through the device. The motion of the particles (electrons) consists of a sequence of free flights ending in collision events, so the trajectories of these particles are random [65]. The standard description of charge transport in semiconductors is given by the Boltzmann Transport Equation (BTE) [67]. The BTE is an integral-differential kinetic equation, which also correctly describes the charge transport in devices where the sizes are lower than De Broglie's wavelength. In general it is not possible to neglect the quantum effects [68]. The study of charge transport properties in a semiconductor in the presence of an external field is not simple, especially when the field is very strong. In fact, in these cases, the BTE does not have an analytical solution. To solve this problem, many assumptions can be made, as in the drift-diffusion model and the hydrodynamic model, where the particles are treated as a fluid. However, the validity of these models is limited and they cannot be applied to most modern devices.

In spite of this, there is an indirect way to solve the problem. Because the electronic current consists of single particles with their own transport sequence, a device can be correctly described by following the motion of each particle. The free flight time and the collision mechanism that causes the end of

free flight are distributed in a stochastic way. By generating pseudorandom numbers with a suitable distribution, it is possible to calculate the motion of each particle and simulate the characteristics of a device [69]-[70]. This method, called Monte Carlo, represents a continuous solution in real space and in the time of Maxwell and Boltzmann's equations, and it is very useful to study the response of a device, both in the presence of static fields or non-stationary fields [71]-[72].

The BTE is an equation of motion for the probability distribution function in the 6-dimensional phase space of position and (crystal) momentum

$$\frac{\partial f(\mathbf{r},\mathbf{k},t)}{\partial t}+\frac{1}{\hbar}\nabla_{\mathbf{k}}E(\mathbf{k})\nabla_{\mathrm{r}}f(\mathbf{r},\mathbf{k},t)+\frac{e\mathbf{F}}{\hbar}\nabla_{\mathbf{k}}f(\mathbf{r},\mathbf{k},t)=\left.\frac{\partial f(\mathbf{r},\mathbf{k},t)}{\partial t}\right|_{Coll}, \quad (1.22)$$

where $f(\mathbf{r},\mathbf{k},t)$ is the one-particle distribution function. The right hand side is the rate of change of the distribution function due to randomizing collisions, and it is an integral over the in-scattering and the out-scattering terms in momentum (wavevector) space. Once $f(\mathbf{r},\mathbf{k},t)$ is known, physical observables, such as average velocity or current, are found through averages over f distribution [67]. Equation (1.22) is semi-classical in the sense that particles are treated as having distinct position and momentum in violation of the quantum uncertainty relations, but their dynamics and scattering processes are quantum-mechanically treated through the electronic band structure and the use of the time dependent perturbation theory [65, 73].

The BTE is still an approximation of the underlying many body Liouville equation from a classical point of view, and of the Liouville-von Neumann equation for the density matrix in a quantum-mechanical framework [74]. The main approximations of the BTE are the assumption of instantaneous scattering processes in space and time, the Markov nature of scattering processes (i.e. that they are uncorrelated with the previous scattering events), and the neglecting of multi-particle correlations (i.e. that the system may be characterized by a single particle distribution function). In semi-classical simulation, some of these assumptions are relaxed through the use of molecular dynamics techniques (in the context of device simulations).

1.4 Monte Carlo Transport Calculation [1]

The Monte Carlo (MC) technique is based on the generation of a random walk in order to simulate the stochastic motion of the particle subject to collision processes in some mediums. This process of random walk generation may be used to evaluate integral equations, and is connected to the general random sampling technique used in the evaluation of multi-dimensional integrals.
The MC algorithm explicitly consists of generating random free flight times for each particle, choosing the type of scattering that occurrs at the end of the free flight, changing the final energy and momentum of the particle after scattering, and then repeating the procedure for the next free flight. The sampling of particle motion at various times throughout the simulation allows the statistical estimation of physically interesting quantities such as the single particle distribution function, the average drift velocity in the presence of an applied electric field, the average energy of the particle, etc. By simulating an ensemble of particles that are representative of the physical system of interest, the non-stationary time-dependent evolution of the electron and hole distributions under the influence of a time-dependent driving force can be simulated.

1.4.1 Single-Particle Monte Carlo Simulation

In general, the analysis of the carrier transport in a semiconductor is a many-body problem with a large number of carriers mutually interacting; hence it is a very difficult task. However, when the many-body system can be considered an ensemble of independent carriers, it becomes possible to use an approximate method that simulates this ensemble of carriers by monitoring the history of a single carrier undergoing many scattering events.
The *Single-particle Monte Carlo* (SMC) method is straightforward and can be carried out without the need to assume the shape of the distribution function. It consists of simulating the motion of a single carrier in the momentum space by stochastically selecting the duration of the carrier free flights and the

scattering events, making a mapping between the probability density of the given microscopic process and a uniform distribution of random numbers.

Free Flight Generation [65]

In the MC method, in order to simulate the motion of a particle with a random walk process, the probability density *P(t)* is required, in which *P(t)dt* is the joint probability that a particle arrives at time t without scattering after the previous collision at $t = 0$, and then undergoes a collision in a time interval dt. The probability of scattering in the time interval dt may be written as $\Gamma[\mathbf{k}(t)]dt$, where $\Gamma[\mathbf{k}(t)]$ is the scattering rate of an electron or hole having wavevector $\mathbf{k}$. The scattering rate, $\Gamma[\mathbf{k}(t)]$, represents the sum of the contributions from each individual scattering mechanism, which is usually calculated using perturbation theory. The implicit dependence of $\Gamma[\mathbf{k}(t)]$ on time reflects the change in $\mathbf{k}$ due to acceleration by internal and external fields. For electrons subject to time independent electric and magnetic fields, the time evolution of $\mathbf{k}$ between collisions is described as

$$\mathbf{k}(t) = \mathbf{k}(0) - \frac{\boldsymbol{e}(\mathbf{F} + \mathbf{v}\times\mathbf{B})t}{\hbar} \tag{1.23}$$

where $\mathbf{F}$ is the electric field, $\mathbf{v}$ is the electron velocity, and $\mathbf{B}$ is the magnetic field. In terms of the scattering rate, $\Gamma[\mathbf{k}(t)]$, the probability that a particle has not undergone a collision after a time t is given by $\exp(-\int_0^t \Gamma[\mathbf{k}(t')]dt')$. Thus, the probability of scattering in the time interval dt after a free flight of time t may be written as the joint probability

$$P(t)dt = \Gamma[\mathbf{k}(t)]\exp\left(-\int_0^t \Gamma[\mathbf{k}(t')]dt'\right)dt. \tag{1.24}$$

Random flight times may be generated according to the probability density *P(t)* by using, for example, a pseudo-random number generator, which generates random numbers uniformly distributed in the range [0,1]. Using a direct method, random flight times can be generated according to

$$r = \int_0^{t_r} P(t)dt, \tag{1.25}$$

where r is a uniformly distributed random number and t_r is the desired free flight time. Integrating (1.25) with *P(t)* given by (1.24) yields

$$r = 1 - \exp\left(-\int_0^t \Gamma[\mathbf{k}(t')]dt'\right). \tag{1.26}$$

Since $1 - r$ is statistically the same as r, (1.26) can be simplified to

$$-\ln r = \int_0^{t_r} \Gamma[\mathbf{k}(t')]dt'. \tag{1.27}$$

Equation (1.27) is the fundamental equation used to generate the random free flight time after each scattering event, resulting in a random walk process related to the underlying particle distribution function. If there is no external driving field leading to a change in **k** between scattering events, the time dependence vanishes, and the integral is trivially evaluated. In the general case where this simplification is not possible, it is a good expedient to introduce the self-scattering method [65], in which a fictitious scattering mechanism is introduced, whose rate always adjusts itself in such a way that the total (self-scattering plus real scattering) rate is a constant in time.

$$\Gamma = \Gamma[\mathbf{k}(t')] + \Gamma_{self}[\mathbf{k}(t')], \tag{1.28}$$

where Γ_{self} $[\mathbf{k}(t')]$ is the self-scattering rate. The self-scattering mechanism is defined in such a way that the final state before and after scattering is identical. Hence, when it is selected as the terminating scattering mechanism, it has no effect on the free flight trajectory of a particle, but allows the simplification of Eq. (1.27) so that the free flight is given by

$$t_r = -\frac{1}{\Gamma}\ln r. \tag{1.29}$$

The constant total rate (including self-scattering) Γ is chosen *a priori* so that it is larger than the maximum scattering encountered during the simulation interval. In the simplest case, a single value is chosen at the beginning of the

entire simulation (constant Γ method), checking to ensure that the real rate during the simulation never exceeds this value.

Final State After Scattering

The algorithm described above determines the random free flight time during which the particle dynamics are semi-classically treated according to Eq. (1.23). For the scattering process, we need the type of scattering (i.e. impurity, acoustic phonon, photon emission, etc.) which terminates the free flight, and the final energy and momentum of the particle after scattering. The type of scattering that terminates the free flight is chosen using a uniform random number between 0 and Γ, which, used as pointer, allows the final energy and momentum of the particle to be selected from among the relative total scattering rates of all the processes, including self-scattering.

$$\Gamma = \Gamma_{self}[n,\mathbf{k}] + \Gamma_1[n,\mathbf{k}] + \Gamma_2[n,\mathbf{k}] + \cdots + \Gamma_N[n,\mathbf{k}], \tag{1.30}$$

where n is the band index of the particle (or subband in the case of reduced dimensionality systems), $\mathbf{k}$ is the wavevector at the end of the free-flight and N is the number of different types of scattering mechanisms. Once the type of scattering that terminates the free flight has been selected, the final energy and momentum (as well as band or subband) of the particle due to this type of scattering must be selected. For this selection, the scattering rate, $\Gamma_j[n, \mathbf{k};m,\mathbf{k}']$, of the j^{th} scattering mechanism is necessary, where n and m are the initial and final band (subband) indices, and $\mathbf{k}$ and $\mathbf{k}'$ are the particle wavevectors before and after scattering. Defining a spherical coordinate system around the initial wavevector $\mathbf{k}$, the final wavevector $\mathbf{k}'$ is specified by $|\mathbf{k}'|$ (which depends on conservation of energy) as well as the azimuthal and polar angles, φ and θ around $\mathbf{k}$. Typically the scattering rate $\Gamma_j[n, \mathbf{k}; m, \mathbf{k}']$ only depends on the angle θ between $\mathbf{k}$ and $\mathbf{k}'$. Therefore, φ may be chosen using a uniform random number between 0 and 2π (i.e. $2\pi r$), while θ is chosen according to the cross-section for scattering arising from $\Gamma_j[n,\mathbf{k}; m,\mathbf{k}']$. If the probability for scattering into a certain angle $P(\theta)d\theta$ is integrable, then random angles satisfying this probability density can be generated by the direct method, through the

inversion of Eq. (1.25). Otherwise, a rejection technique can be used to select random angles according to *P(θ)*.

1.4.2 Scattering Process

In the scattering calculation**,** we first select a scattering mechanism by which an electron is to be scattered, and then identify the electron state after scattering.

Fig. 1.8 lists the scattering mechanisms one should consider in a typical MC simulation. They are roughly divided into scattering due to crystal defects, which is primarily elastic in nature, lattice scattering between electrons (holes) and lattice vibrations or phonons, which are inelastic. Phonon scattering involves different modes of vibration, either acoustic or optical, as well as both transverse and longitudinal modes. Carriers may either emit or absorb quanta of energy from the lattice, in the form of phonons, in individual scattering events. The designation of inter- versus intra-valley scattering comes from the multi-valley band structure model, and refers to whether the initial and final states are in the same valley or in different valleys.

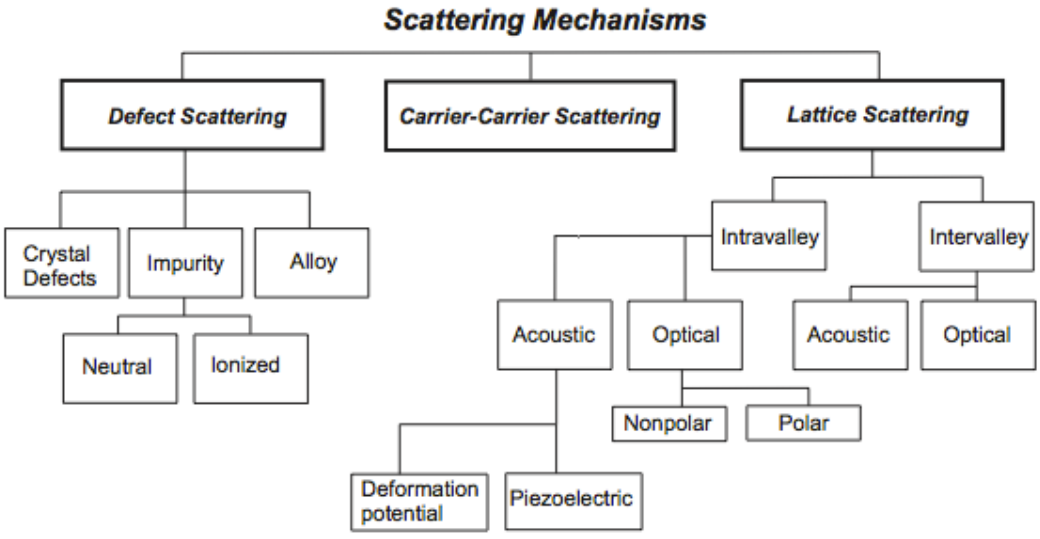

Figure 1.8: Scattering mechanisms in a typical semiconductor.[66]

The selection of a scattering mechanism *(n)* can be made by using functions

$\Lambda_n(E_\mathbf{k})$ defined as

$$\Lambda_n(E_\mathbf{k}) = \frac{\sum_{j=1}^{n} W_j(E_\mathbf{k})}{\Gamma} \qquad \text{for } n = 1, 2, \ldots, N \tag{1.31}$$

which are the successive summations of the scattering rates normalized with Γ. Γ is identical to the parameter defined by (1.28), and N is the total number of scattering mechanisms. A scattering mechanism for an electron with energy $E_\mathbf{k}$ is selected by generating a random number r_2 lying between 0 and 1, and comparing it to $\Lambda_n(E_\mathbf{k})$; thus, the n-th scattering mechanism is chosen if the condition given by

$$\Lambda_{n-1}(E_\mathbf{k}) < r_2 < \Lambda_{n-1}(E_\mathbf{k}) \qquad n = 1, 2, \ldots, N \tag{1.32}$$

is satisfied.

Having determined the scattering mechanism, we next determine the wave vector **k'** after scattering. The magnitude of **k'** is known by the energy conservation. The direction of **k'** needs to be determined in terms of its components in a Cartesian coordinate $\left(k_x^L, k_y^L, k_z^L\right)$ according to the *laboratory frame* (x^L, y^L, z^L) chosen for the simulated device. If the scattering is isotropic (i.e., if the scattered electron has the same probability of being in any direction after scattering), the components k_x', k_y' and k_z' can be found by considering that the probability density $p(f',q')df'dq'$ is proportional to the number of available states on a sphere of radius k', where f' and q' are the azimuthal and polar angles of k' in relation to k_z^L. $p(f',q')$ equals $sin\theta'$, since any f' is equally probable. Therefore, f' and q' can be determined by a couple of uniform random numbers, r_3 and r_4, between 0 and 1.

$$\phi' = 2\pi r_3$$

$$\cos\theta' = 1 - 2r_4 \tag{1.33}$$

For f' and q' given by (1.39), the components of the laboratory frame $\left(k_x^L, k_y^L, k_z^L\right)$ are readily obtained as

$$k_x' = k' sin\theta' cos\phi'$$

$$k'_y = k' sin\theta' sin\phi'$$

$$k'_z = k' cos\theta' \tag{1.34}$$

These expressions are only valid in the case of isotropic scattering.

For anisotropic scattering processes, such as impurity scattering and polar optical phonon scattering, determination of θ and ϕ, the polar and azimuthal angles of **k**' in relation to the initial wave vector **k**, is more complicated [see ref. 65].

To calculate the scattering rates in a quasi-two-dimensional electron gas the matrix elements have to be properly calculated for the subband wave functions.

1.4.3 Velocity Calculation

If we accumulate the flight time (or visiting time) of an electron in each volume element of *k*-space, we are able to figure out the distribution function by which the mean carrier velocity and energy can be calculated. This procedure requires a large amount of memory to accumulate the data in c-space. However, it is not necessary to do this, because the mean values of velocity and energy can be calculated directly by monitoring each electron flight and then taking an average over all the flights.

The instantaneous carrier velocity is given by

$$\boldsymbol{v} = \frac{1}{\hbar} \nabla_{\mathbf{k}} E_{\mathbf{k}} \tag{1.35}$$

Therefore, the mean carrier velocity during flight time *t* can be written as

$$\langle \boldsymbol{v} \rangle_{\mathbf{r}} = \frac{1}{\hbar} \frac{\Delta E_{\mathbf{k}}}{\Delta \mathbf{k}} \tag{1.36}$$

where ΔE_k and Δk are small increments of the carrier energy and wave vector during t, respectively. The increment of electron wave vector under a constant electric field is given by

$$\Delta \mathbf{k} = -\frac{e\mathbf{F}}{\hbar} \tau \tag{1.37}$$

Substituting (1.37) with (1.36), we have

$$\langle \boldsymbol{v} \rangle_{\mathbf{r}} = -\frac{\Delta E_{\mathbf{k}}}{e\mathbf{F}\tau} \tag{1.38}$$

Making use of the mean carrier velocity during **r** given by (1.38), the mean carrier velocity during the total simulation time T is obtained as

$$\langle \boldsymbol{v} \rangle_{\mathbf{T}} = \frac{1}{T}\sum \langle \boldsymbol{v} \rangle_{\mathbf{r}} \boldsymbol{\tau} = -\frac{1}{e\mathbf{F}\tau}\sum \Delta E_{\mathbf{k}}$$

$$= -\frac{1}{e\mathbf{F}\tau}\sum (E_{\mathbf{f}} - E_{\mathbf{i}}) \tag{1.39}$$

where E_i, is the carrier energy at the start of the electron flight and E_f, is the energy at the end of the flight. The summation has to be made for all free flights. Equation (1.39) shows that we need to accumulate the energy increment during each free flight. The same reasoning leads to mean carrier energy $\langle E \rangle_T$ being derived as

$$\langle E \rangle_T = \frac{1}{T}\sum \langle E \rangle_\tau \tau \tag{1.40}$$

where $\langle E \rangle_\tau$ is given, with a good approximation, by

$$\langle E \rangle_\tau = \frac{E_i + E_f}{2} \tag{1.41}$$

1.5 Ensemble Monte Carlo

The algorithm described in the previous section can be used to track a single particle over many scattering events, in order to simulate the steady-state behaviour of a system. Transport transient or spin relaxation simulations require the use of a synchronous ensemble of particles in which the algorithm described above is repeated for each particle in the ensemble that represents the system of interest, until the simulation is completed.

The conventional *Ensemble Monte Carlo* (EMC) scheme used for electronic devices describes transport of classical representative particles, called superparticles. Usually, each simulated particle represents a group of real

electrons or holes with similar characteristics. In simulation, each particle is simulated as an SMC procedure described above.

Fig. 1.9 illustrates an EMC simulation in which at fixed time-step Δt, the motion of all the carriers in the system is synchronized. The yellow symbols illustrate random, instantaneous, scattering events, which may or may not occur during one time-step. In this picture, τ indicates the random flight time of an individual electron. Basically, each carrier is simulated only up to the end of the time-step, and then the next particle in the ensemble is dealt with. Within each time-step, the motion of each particle of the ensemble is simulated independently of the other particles.

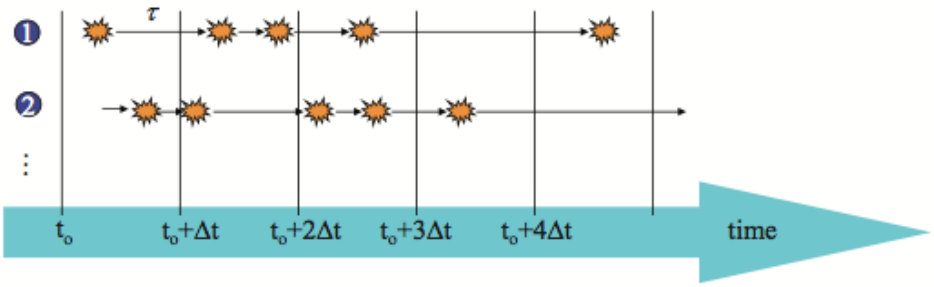

Figure 1.9: Ensemble Monte Carlo simulation in which, the motion of particles is synchronized at each time-step Δt. The yellow symbols represent scattering events.

Nonlinear effects such as carrier-carrier interactions are then updated at each scattering event, as discussed in more detail below. The non-stationary one-particle distribution function and related quantities such as drift velocity, valley or subband population, etc., are then taken as averages over the ensemble at fixed time-steps throughout the simulation.

For example, the drift velocity in the presence of the field is given by the ensemble average of the i-component of the velocity at the n^{th} time step as

$$\bar{v}_i\left(n\Delta t \cong \frac{1}{N}\sum_{j=1}^{N} v_i^j(n\Delta t)\right), \tag{1.42}$$

where N is the number of simulated particles and j labels the particles in the ensemble. This equation represents an estimator of the true velocity, which has a standard error given by

$$s = \frac{\sigma}{\sqrt{N}}, \tag{1.43}$$

where σ^2 is the variance which may be estimated from

$$\sigma^2 \cong \frac{N}{N-1}\left\{\frac{1}{N}\sum_{j=1}^{N}\left(v_i^j\right)^2 - \bar{v}_i^2\right\}. \tag{1.44}$$

Similarly, the distribution functions for the carriers, electrons and holes, may be tabulated by counting their number in cells of **k**-space. From Eq. (1.43), we see that the error in estimated average quantities decreases as the square root of the number of particles in the ensemble, implying the simulation of many particles. Typical ensemble sizes for good statistics are in the range of 10^4-10^5 particles.

1.6 Energy band structure, scattering mechanisms and physical parameters used in our simulations

The transport of the electrons in the Si bulk is simulated by using a single-particle Monte Carlo algorithm, while spin relaxation is calculated by means of an ensemble Monte Carlo code.

The conduction band of silicon is represented by six equivalent X valleys along the ⟨100⟩ directions, approximated as ellipsoids with rotational symmetry, and two effective longitudinal m_L and transverse m_T masses. Because the energy gap between the X and L valley is large (1.05 eV), higher valleys and impact ionization are not taken into account, since for the employed electric field, the electrons do not reach sufficient kinetic energies for these transitions. The code includes both the intervalley and intravalley scattering of electrons in multiple energy valleys. In particular, the scattering by acoustic phonons is taken into account, employing a deformation potential. Ionized impurity scattering is included under the Brooks–Herring approximation and the

intervalley scattering is accounted for by considering six types of optical phonon, three concerning transitions between perpendicular valleys (f-type) and three between parallel valleys (g-type). The scattering probabilities are calculated by using the Fermi Golden Rule and the scattering events are considered instantaneous.

In the silicon MOS inversion layer, the simplification and assumption made in the Monte Carlo procedure are as follows:

- The six equivalent X-valleys are assumed to be spherical and parabolic; therefore, the subband energy levels are the same for all equivalent valleys.
- The potential profile perpendicular to the MOS inversion layer is assumed to be a triangle (triangle potential approximation.
- The scattering processes takes into account the scattering mechanism with intra- and inter- subbands, and non-polar optical and acoustic phonons. This choice is made to avoid numerical integration in the determination of the electron states after scattering.
- The 2DEG is assumed to be non-degenerate

For all the numerical simulations discussed in this thesis scattering probabilities are assumed to be field-independent; accordingly, the influence of the external fields is only indirect through the field-modified electron velocities. At this stage, we neglect the electron–electron interactions and consider electrons as being independent particles. We have also used the parameters of the silicon shown in Table 1.1.

Density, kg/m^{-3}	2329
Longitudinal sound velocity, m/s	9180
Transverse sound velocity, m/s	4700
Lattice dielectric permeability	11.70
	X valley
Electron effective mass:	
longitudinal	$0.9m_0$
transverse	$0.19m_0$
Nonparabolicity coefficient, eV^{-1}	0.5
Number of equivalent valleys	6
Acoustic deformation potential, eV	9

Phonon parameters for electron scattering in silicon

Phonon type	Phonon energy, meV	Electron–phonon coupling constant, 10^{10} eV/cm
f	18.1	0.5
f	43.1	0.8
f	54.3	3.0
g	12.1	0.15
g	18.1	3.4
g	60.3	4.0

Table 1.1:_ Set of *n*-type Si parameters used in the calculations [75]

All results were obtained in Si with a free electron concentration 10^{13} cm^{-3} (nondegenerate low-doped n-type). We assume that all donors are ionized and that the free electron concentration is equal to the doping concentration.

Chapter 2

Semiconductor Noise

Noise in semiconductor devices has a significant impact on circuit's performances. This is even more important in today's low-voltage, high-performance, mixed-signal and RF designs. The capability to measure and characterize semiconductor device noise is a fundamental requirement for design. Noise characterization is also important to monitor the quality of semiconductor processes.

Previous studies have shown that, under specific conditions, an external noise can constructively interact with an intrinsically nonlinear system, characterized by the presence of intrinsic noise, giving rise to positive effects [22]-[24] such as stochastic resonance (SR) [25]-[28], resonant activation (RA) [29, 30] and noise enhanced stability (NES) [32]-[36]. In particular, the possibility of suppressing the intrinsic noise in n-type GaAs and Si bulk, driven by a static electric field, with the addition of a Gaussian correlated noise source, has been theoretically investigated [37]. This section is devoted to the introducing some background knowledge about the concept of noise.

2.1 General Formulation of Noise

In semiconductor devices the current conduction is the result of the flow of discrete charged particles, the electrons. While from a macroscopic point of view the electrons are moving at an average rate in, response to the conditions

within the device, they are fluctuating in their velocity and position due to scattering events, recombination, or trapping and de-trapping of carriers [77].
The motion of electrons in the presence of an electric field is characterized by an average velocity, which depends on the external parameters of the system, such as the amplitude of the applied field and its frequency. The fluctuations of electron velocity around its mean value correspond to the intrinsic noise of the system.
If the applied field is static, the correlation function $C_{\delta v \delta v}(\tau)$ of the velocity fluctuations can usually be calculated as:

$$C_{\delta v \delta v}(\tau) = \langle \delta v(t) \delta v(t + \tau) \rangle = \langle v(t) v(t + \tau) \rangle - \langle v(t) \rangle^2, \quad (2.1)$$

in which τ is the correlation time and the average is done over a sequence of a long enough time interval $[0; T]$.
For systems operating under cyclostationary conditions, the correlation function $C_{\delta v \delta v}(t,\tau)$ of the velocity fluctuations $\delta v(t) = v(t) - \langle v(t) \rangle$ can be calculated [55] as

$$C_{\delta v \delta v}(t, \tau) = \langle v\left(t - \frac{\tau}{2}\right) v\left(t + \frac{\tau}{2}\right) \rangle - \langle v\left(t - \frac{\tau}{2}\right) \rangle \langle v\left(t + \frac{\tau}{2}\right) \rangle \quad (2.2)$$

in which τ is the correlation time and the average is calculated over a sequence of equivalent time instants $t = s + mT$, with s belonging to the time interval $[0, T]$ (T is the field period) and m is an integer [55]. This two-time symmetric correlation function eliminates any regular contribution and describes only the fluctuating part of *v(t)*. By averaging over the whole set of values of t within the period T, the velocity autocorrelation function becomes

$$C_{\delta v \delta v}(\tau) = \frac{1}{T} \int_0^T C_{\delta v \delta v}(t, \tau) dt \quad (2.3)$$

According to the Wiener–Kintchine theorem, the spectral density can be calculated as the Fourier transform of $C_{\delta v \delta v}(\tau)$.

2.2 Classification of Intrinsic Noise

There are several sources causing fluctuations in time-varying currents: thermal noise, 1/f noise, generation-recombination noise and quantum noise. In terms of frequency behaviour, distinct trends can be identified.

Some noise is constant over some frequency ranges, whereas other noise diverges as frequency decreases.

Fig. 2.1 shows the different types of noise that may be observed at a contact of a semiconductor device.

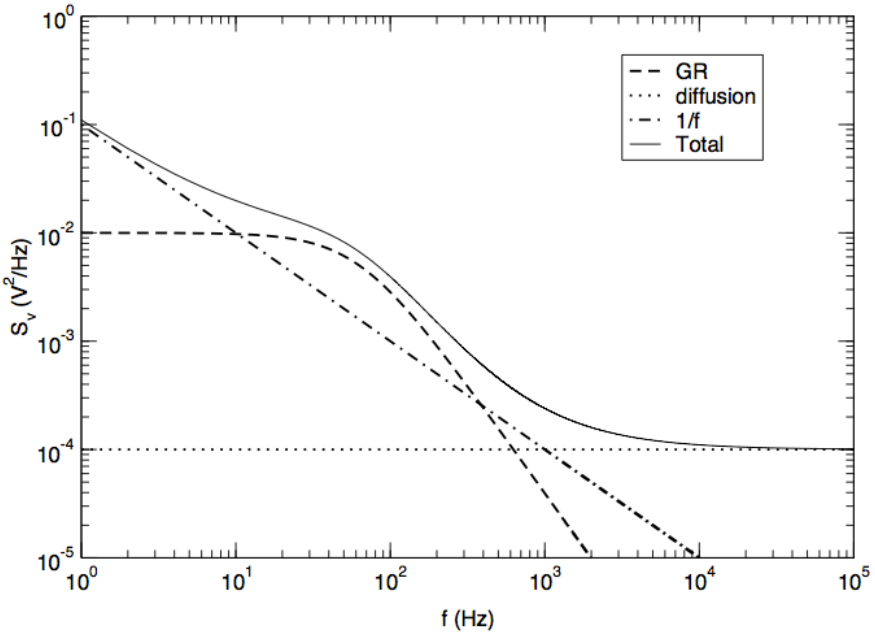

Figure 2.1: Types of noise

2.2.1 Low-frequency noise sources

The Generation-recombination (GR) and 1/f noise components in Figure 2.1 are referred to as low-frequency noise because their spectral density rolls off with increasing frequency. The (GR) noise is due to fluctuations in the number of free carriers inside a two-terminal sample associated with random transitions of charge carriers between states in different energy bands. Accordingly, it represents a typical noise source in semiconductor materials, where carrier concentration can vary over many orders of magnitude. Typical examples of

transitions are between conduction band and localized levels in the energy gap, conduction and valence bands, etc. [79]

Therefore, GR noise is inherently due to fluctuations in the carrier number, usually maintaining the charge neutrality of the total sample. The GR noise has a Lorentzian spectrum of the form [80]

$$S_i = \frac{B\tau}{1 + (2\pi f\tau)^2} \tag{2.4}$$

where τ is a time-constant and B has a dependence on the current flowing through the device.

The 1/f noise has several alternative names, for example, flicker noise, pink noise or telegraph noise. The 1/ f noise component is typically characterized by a current spectral density [81]

$$S_i = \frac{K_F I^{A_F}}{f} \tag{2.5}$$

and is associated with a superposition of Lorentzian spectra or current-density fluctuations [82] with a microscopic spectral density of

$$S_i = \frac{\alpha_H J^2}{f_n} \tag{2.6}$$

where α_H is a phenomenological parameter based on mobility fluctuations, n is the number of carriers, and J is the current density.

2.2.2 White noise sources

Two common noise quantities considered in semiconductor devices are thermal and shot noise, shown as diffusion noise in Figure 2.1. These noise sources are also referred to as being white because they have equal power at every frequency up into the THz region. Thermal noise for a resistor is characterized by

$$S_i = \frac{4kT}{R} \tag{2.7}$$

where S_i is the current spectral density, k is Boltzmann's constant, T is the temperature of the device, and R is the resistance in ohms. For a diode, shot noise is characterized as

$$S_i = 2qI \tag{2.8}$$

where q is the charge of an electron and I is the current flowing through the device. While these noise sources appear to be different, with Equation 2.7 having no bias dependence and Equation 2.8 having a current dependence, they result from the same microscopic fluctuation. The spectral density of this fluctuation [77] is

$$S = 4q^2 D_\alpha \alpha \frac{\partial y \partial z}{\partial x} \tag{2.9}$$

where $\alpha = n, p$ is the electron and hole density respectively, and D_α is the diffusivity.

2.2.3 Quantum Noise

Quantum noise is the frequency-dependent excess noise. It is proportional to the frequency, becoming the dominant fluctuations at high frequencies (see Fig. 2.2).

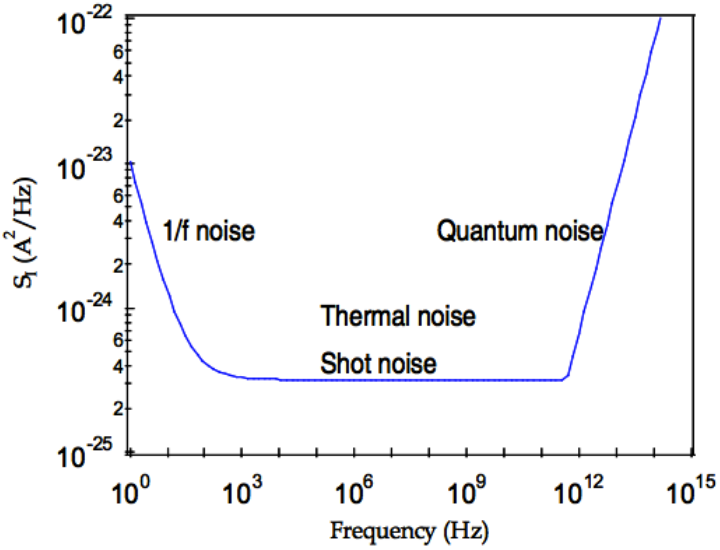

Figure 2.2: Spectrum of dominant noise sources in frequency domain

To describe quantum noise, correlations between electrons originating from Coulomb interactions and the Pauli exclusion principle should be considered similar to shot noise. Furthermore, I, i.e. quantum noise, includes vacuum fluctuations. The finite frequency current spectral density is written with energy-independent transmission probabilities T_n

$$S_I(f) = \sum_n^N T_n(1-T_n)\frac{2e^2}{\hbar}\left[(eV+hf)\coth\left(\frac{eV+hf}{2k_BT}\right)+(eV-hf)\coth\left(\frac{eV-hf}{2k_BT}\right)\right] + \sum_n^N T_n^2\frac{2e^2}{h}\left[2hf\coth\left(\frac{hf}{2k_BT}\right)\right]. \quad (2.10)$$

It is reduced to a simple form $S_I = 2hfG$ in the limit where $hf \gg eV,\ k_BT$ with G= $2e^2/h\sum T_n$. Equation (2.10) is a complete and general form of the current spectral density including shot noise, thermal noise and quantum noise.

2.3 External noise source

Recently, an increasing interest has been directed towards the constructive aspects of noise in the dynamic response of non-linear systems. Several studies have investigated hot-electron transport dynamics in bulk and semiconductor structures by analysing the electronic noise in systems driven by external static or oscillating electric fields [4]-[21] containing time-correlated fluctuations [34, 35], or a two-level random telegraph noise source [36]

2.3.1 Gaussian correlated source of noise

In the case of Gaussian correlated noise, the random component of the electric field η(t) is modelled as an Ornstein-Uhlenbeck (OU) process, which obeys the stochastic differential equation [83]

$$\frac{d\eta(t)}{dt} = -\frac{\eta(t)}{\tau_D} + \sqrt{\frac{2D}{\tau_D}}\xi(t) \quad (2.11)$$

where τ_D and D are, respectively, the correlation time and the intensity of the noise described by the OU process which has an autocorrelation function expressed by

$$\langle \eta(t)\eta(t') \rangle = D\, exp(-\frac{|t - t'|}{\tau_D}). \tag{2.12}$$

ξ(t) is a Gaussian white noise with zero mean < ξ(t) >= 0, and autocorrelation function

$$\langle \xi(t)\xi(t') \rangle = \delta(t - t'). \tag{2.13}$$

Within the framework of Ito's calculus, the general solution of equation (2.12) leads to the following complete expression for the stochastic evolution of the amplitude of the electric field

$$F(t) = F_0 + \eta(0)e^{-t/\tau_D} + \sqrt{\frac{2D}{\tau_D}} \int_0^t e^{-\frac{t-t'}{\tau_D}} dW(t') \tag{2.14}$$

where the initial condition is η(0) = 0, and W (t) is the Wiener process [83]. In a practical system, η(t) could be generated by a RC circuit driven by a source of Gaussian white noise, with correlation time $\tau_D = (RC)-1$ (see equation (2.11)). The Gaussian white noise can be generated by the Zener breakdown phenomenon in a diode, in an inversely polarized base-collector junction of a BJT, or by amplifying the thermal noise in a resistor [84]. The correlation time τ_D is tunable by using a diode (varicap) with a voltage-dependent variable capacitance; the noise intensity D can be chosen, for example, by suitably amplifying the noise produced through the Zener stochastic process.

2.3.2 Random Telegraph noise

In the case of random telegraph or dichotomous noise (DM), η(t) is generated by a random process taking only discrete values and stochastically switching between these values. Let us consider a symmetric dichotomous Markovian stochastic process with only two values [85, 90] $\eta(t) \in \{-\Delta, \Delta\}$. Thus, we have a

zero mean $\langle \eta(t) \rangle = 0$, and correlation function

$$\langle \eta(t)\eta(t') \rangle = \Delta^2 \, exp(-\frac{|t - t'|}{\tau_D}). \tag{2.15}$$

where τ_D is the correlation time of the noise. It is related to the inverse of the mean frequency of transition from $\pm\Delta$ to $\mp\Delta$, respectively.

In our runs, we choose $\eta(0) = X$ as the initial condition, where X is a random variable which takes the values $-\Delta$ and Δ with equal probability ($p = 1/2$). We only consider fluctuations of equal height, in such a way that this external noise can easily be generated in practical systems, and tuning effects can be more controllable. A dichotomous Markovian noise can be realized, for example, by means of a cheap and simple home-made noise generator, based on the generation of a pseudo-random sequence by a linear-feedback shift register SR2.

2.4 Semiconductor noise calculation in the presence of a fluctuating electric field

The noise-induced changes of intrinsic noise properties are investigated by a statistical analysis of the autocorrelation function of the velocity fluctuations and its mean spectral density. Although the single excitation is not periodic due to the presence of the random component, our process exhibits cyclostationarity since its average statistical properties vary cyclically with time, i.e.

$$\langle F(t + mT) \rangle = \langle F(t) \rangle$$
$$\langle v(t + mT) \rangle = \langle \langle v(t) \rangle, \tag{2.16}$$

where the brackets $\langle \ldots \rangle$ mean the average over an ensemble of different realizations of F(t) and v(t) histories.

In the computations of the autocorrelation function we have considered 10^3 possible initial values of s and a total number of equivalent time instants $m \cong 10^6$.

2.4.1 Analytical Theory of Noise suppression

The average electron velocity is modified by the presence of an external source of noise [37]. In particular, assuming that the characteristic time scale of the intrinsic fluctuations is much smaller than any other characteristic time of the system enables the correlation function to be approximated by a delta function as

$$C(\tau, E) = S(E)\delta(\tau), \tag{2.17}$$

where *S(E)* is the low frequency value of the spectral density of velocity fluctuations. Under the assumptions that the time τ_D is long enough for the system to follow the variations of *E(t)* and that $\langle \delta E^2 \rangle$ is small, the main result of the theory can be summarized in the following two formulas:

$$\langle v(E_0) \rangle_0 = \langle v(E_0) \rangle + \frac{1}{2} \frac{d^2 \langle v(E_0) \rangle}{dE^2} \langle \delta E^2 \rangle \tag{2.18}$$

and

$$S_0(E_0) = S(E_0) + \left\{ 2\tau_F \left[\frac{d\langle v(E_0) \rangle}{dE} \right]^2 + \frac{1}{2} \frac{d^2 S(E_0)}{dE^2} \right\} \langle \delta E^2 \rangle \tag{2.19}$$

where the subscript 0 means averaging in the presence of external noise. The former relation indicates that the average velocity is modified by the presence of the external noise, but the most interesting result is given by the latter equation which demonstrates that the intrinsic noise of the system can be reduced if the term $d^2S(E_0)/dE^2$ is negative and the characteristic time of the fluctuations of the electric field τ_D is small enough.

Chapter 3

External Noise Effects in Silicon Mos Inversion Layer

In this chapter we investigate the effect of the addition of an external source of correlated noise on the electron transport in a silicon MOS inversion layer, driven by a static electric field. In our modelling of the quasi-two-dimensional electron gas, the potential profile, perpendicular to the MOS structure, is assumed to follow the triangular potential approximation. We calculate the changes in both the autocorrelation function and the spectral density of the velocity fluctuations, for different values of noise amplitude and correlation time.

3.1 MOS modeling

Quantum-confined semiconductor-based devices, such as silicon MOS, are the cornerstone of current electronics. In these structures, spatial confinement leads to the formation of discrete low-dimensional subbands. Energy levels are quantized in each direction of confinement, while the momentum remains a good (continuous) quantum number in the unconfined directions [66]. For a given energy in the conduction band, the allowed electron wavevectors trace out a surface in **k**-space. In the effective-mass approximation for silicon, these constant energy surfaces can be visualized as six equivalent ellipsoids of revolution (Fig.

3.1), whose major and minor axes are inversely proportional to their effective masses. A collection of such ellipsoids for different energies is referred to as a valley.

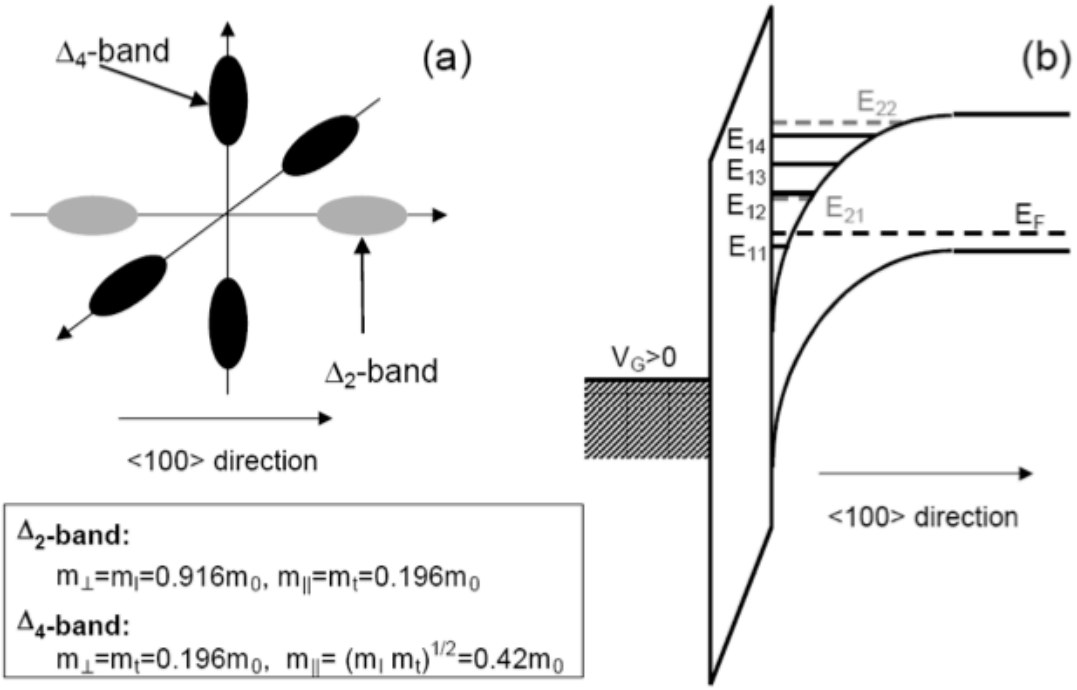

Figure 3.1. (a) Constant-energy surfaces for the conduction-band of silicon, showing six conduction-band valleys in the ⟨100⟩ direction of momentum space. (b) Potential diagram for inversion of p-type silicon.

The band minima, corresponding to the centers of the ellipsoids, are 85% of the way to the Brillouin-zone boundaries. The long axis of an ellipsoid corresponds to the longitudinal effective mass of the electrons in silicon, m_l = 0.916 m_0, while the short axes correspond to the transverse effective mass, m_t = 0.190 m_0 (m_0 is the free-electron mass). For a ⟨100⟩ surface, the Δ_2-band has the longitudinal mass (m_l) perpendicular to the semiconductor interface and the Δ_4-band has the transverse mass (m_t) perpendicular to the interface. Since larger mass leads to a smaller kinetic term in the Schrödinger equation, the unprimed lader of subbands (as it is usually called), corresponding to the Δ_2-band, has the lowest ground state energy. The degeneracy of the unprimed ladder of subbands for a ⟨100⟩ surface is 2. For the same reason, the ground state of the primed ladder of subbands corresponding to the Δ_4-band is higher than the lowest subband of the unprimed ladder of subbands. The degeneracy of the

primed ladder of subbands for a ⟨100⟩ surface is 4.

Here, the silicon inversion layer is modeled as a triangular potential well, i.e. $E_c(z) = eEz,\ z \geq 0$ [66, 87]. Then the subband wavefunctions $\psi_n(z)$ satisfy the one-dimensional Schrödinger equation

$$-\frac{\hbar^2}{2m_0}\frac{\partial^2\psi(z)}{\partial z^2} + eEz\psi(z) = E_n\psi(z) \tag{3.1}$$

where E_n is the subband energy.

We have determined both energy levels and wave functions by using the variational method based on the minimization of the energy eigenvalue of the following approximate wavefunctions [65]:

$$\psi_1(z) = k_1 z \exp\left(-\frac{c_1 z}{2}\right)$$

$$\psi_2(z) = k_2(z + a_2 z^2) \exp\left(-\frac{c_2 z}{2}\right)$$

$$\psi_3(z) = k_3(z + a_3 z^2 + b_3 z^3) \exp\left(-\frac{c_3 z}{2}\right) \tag{3.2}$$

where a_n, b_n, c_n and k_n (with n = 1, 2, 3) are the variational constants to be determined;, and k_n is the normalization constant.

The requirement in the variational method is the minimization of the energy eigenvalue:

$$E_n = \int_0^\infty \psi_n^* H \psi_n \, dz \rightarrow min \tag{3.3}$$

The conditions for the normalization and orthogonality of the wave functions are also given as

$$\delta_{m,n} = \int_0^\infty \psi_m^* \psi_n \, dz \tag{3.4}$$

where $\delta_{m,n}$ is the Kronecher delta.

Substituting 3.2 into 3.3, we have the following energy eigenvalue:

$$E_n = K_n^2 \left\{ \frac{\hbar^2}{2m^*} \left(\frac{1}{2c_n} + \frac{a_n}{c_n^2} + \frac{2a_n^2}{c_n^3} + \frac{12a_n b_n}{c_n^4} + \frac{36b_n^2}{c_n^5} \right) + \right.$$

$$+ eF\left(\frac{6}{c_n^4}+\frac{84a_n}{c_n^5}+\frac{120(a_n^2+2b_n)}{c_n^6}+\frac{1440a_nb_n}{c_n^7}+\frac{5040b_n^2}{c_n^8}\right)\Bigg\} \qquad (3.5)$$

the normalization constant can also be found from (3.4)

$$K_n=\frac{1}{\sqrt{\frac{2}{c_n^3}+\frac{12a_n}{c_n^4}+\frac{24(a_n^2+2b_n)}{c_n^5}+\frac{240a_nb_n}{c_n^6}+\frac{720b_n^2}{c_n^7}}} \qquad (3.6)$$

where we have to set *n=1* and $a_n=b_n=0$ for the ground state subband, *n=2* and $b_n=0$ for the second subband, and *n=3* for the third subband, respectively, in (3.5) and (3.6). For example, we have the following simple form for the energy level and the normalization constant for the ground state subband:

$$E_1=\frac{\hbar^2}{2m^*}\left(\frac{c_1}{2}\right)^2+\frac{3eE}{c_1} \qquad (3.7)$$

$$K_1=\sqrt{\frac{c_1^3}{2}} \qquad (3.8)$$

The value of c_1, which minimizes E_1, is readily found as

$$\mathrm{c_1}=\sqrt[3]{\frac{12\mathrm{m^*eE}}{\hbar^2}} \qquad (3.9)$$

The orthogonality of the second subband wave function to that of the ground state results in the following relations between the coefficients:

$$a_2=-\frac{1}{6}(c_1+c_2) \qquad (3.10)$$

Substituting (3.10) with (3.5) to eliminate a_2 from the energy eigenvalue E_2, it can be expressed as a function of only c_2, and we can find the value of c_2, which minimizes E_2, numerically.

The ortogonality of the ground state and second subbands gives the following relations:

$$a_3 = -\frac{1}{3}\left[\frac{A^2(B+5a_2) - B^2(B+3a_2)}{A(B+5a_2) - B(B+4a_2)}\right] \tag{3.11}$$

$$b_3 = \frac{AB}{12}\left[\frac{A(B+4a_2) - B(B+3a_2)}{A(B+5a_2) - B(B+4a_2)}\right] \tag{3.12}$$

where

$$\mathrm{A} = \frac{\mathrm{c}_1 + \mathrm{c}_3}{2}, \qquad \mathrm{B} = \frac{\mathrm{c}_2 + \mathrm{c}_3}{2} \tag{3.13}$$

Substituting 3.12 into 3.5, the energy eigenvalues for the third subband can be expressed as a function of c_3. We can numerically determine the value of c_3 that minimizes the energy level of the third subband.

The Q2DEG is driven by a fluctuating electric field directed along the x-axis:

$$\mathrm{E(t)} = \mathrm{E} + \eta(\mathrm{t}) \tag{3.14}$$

where E is the amplitude of the deterministic part and η(t) is the random term modelled by an Ornstein-Uhlenbeck (OU) stochastic process (see equation 2.11).

With the aim of finding the most favourable conditions for noise suppression in silicon Q2DEG, we have preliminarily calculated S_0 at T=77K and T=300K.

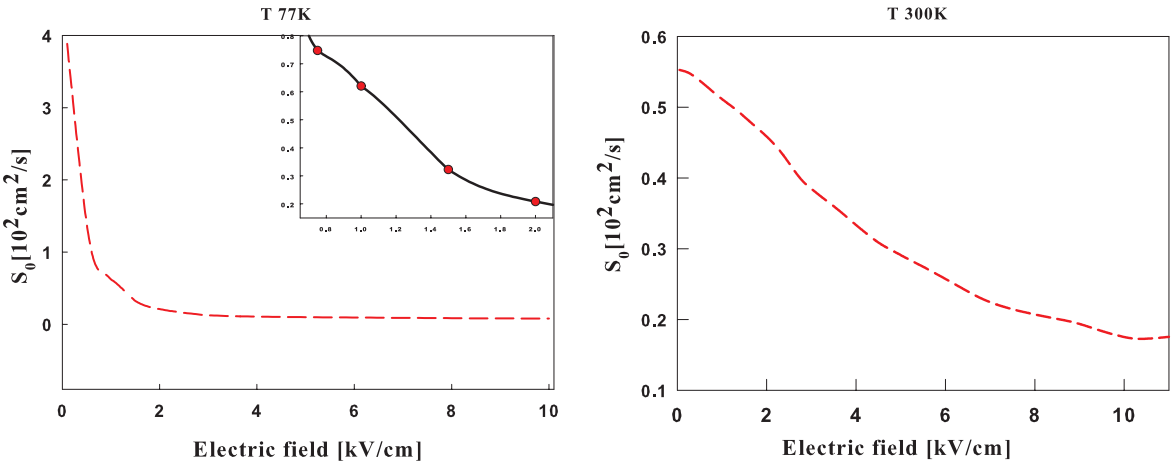

Figure 3.2: Spectral density of the velocity fluctuations at zero frequency (S_0) as a function of the electric field calculated by the Monte Carlo simulation at temperature T =77K and T=300K in Q2DEG SiMOS.

In Fig. 3.2, at T=300K, we can see that S_0 exhibits a maximum at zero field, thus implying a negative $d^2S(E_0)/dE^2$ in the low field region, which is a necessary condition to obtain noise suppression. Furthermore, the spectral density S_0 reaches a minimum at E = 10 kV/cm. At T=77K, S_0 shows a negative $d^2S(E_0)/dE^2$ in the low field region.

3.2 Results and discussion [88]

For the purpose of confirming the validity of the analytical theory in silicon Q2DEG, and investigating the role of τ_D in the suppression of noise, we initially investigated the transport electron dynamics in the presence of a static electric field with an amplitude of E = 10 kV/cm.

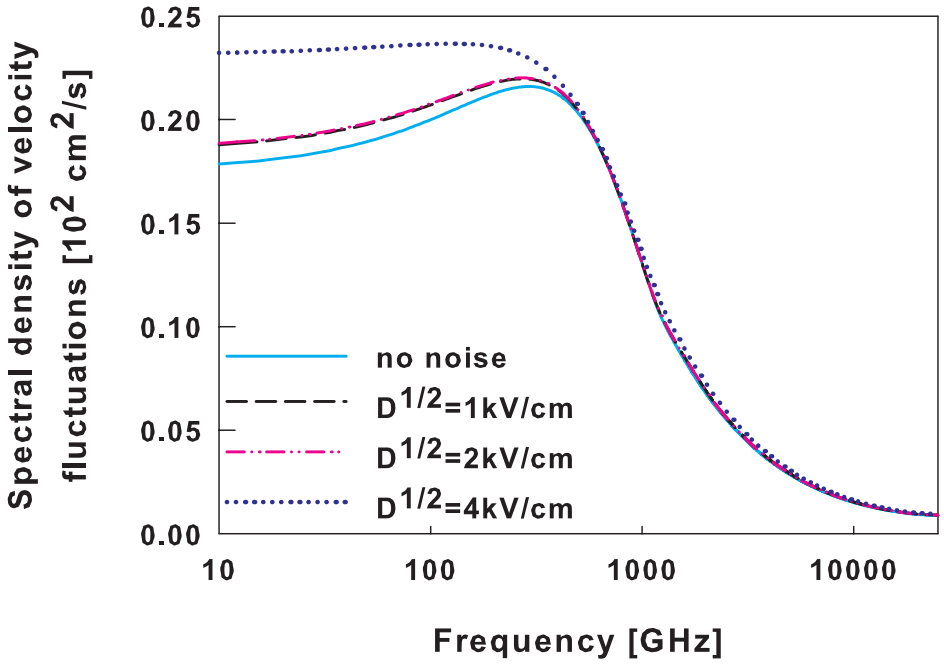

Figure 3.3: Spectral densities of the velocity fluctuations obtained for a static electric field E = 10 kV/cm and the addition of a correlated source of noise, characterized by τ_D = 2 ps for three different values of noise intensity D.

In order to elucidate the effects of the correlated noise source on the intrinsic noise properties, we performed 100 different realizations and evaluated both average values and error bars for the calculated integrated spectral densities.

Fig. 3.3 shows the spectral densities of the velocity fluctuations obtained by adding a source of correlated noise, characterized by τ_D=2 ps for three different values of noise amplitude $D^{1/2}$ (namely $D^{1/2}$ = 1, 2 and 4kV/cm).

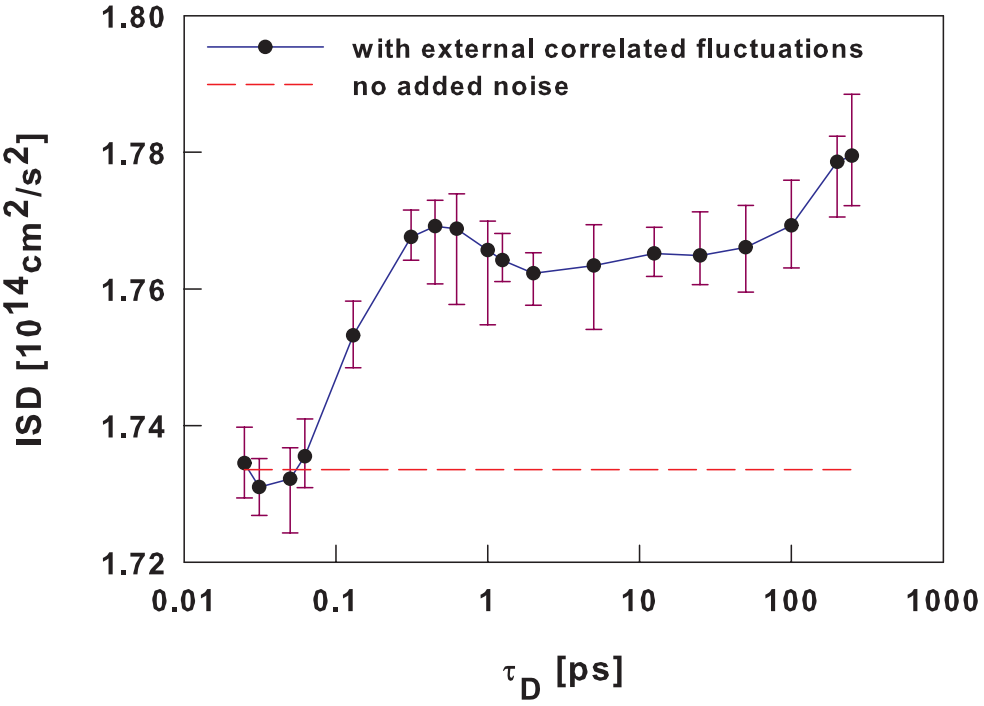

Figure 3.4: ISD of the velocity fluctuations obtained with a static electric field E = 10 kV/cm and the addition of a source of correlated noise with an amplitude of $D^{1/2}$ = 2 kV/cm for different values of the noise characteristic time τ_D. The dashed line represents the ISD obtained in the absence of external noise.

Fig. 3.4 shows the integral spectral density (ISD) of the velocity fluctuations obtained with E = 10 kV/cm and a source of correlated noise with $D^{1/2}$ = 2 kV/cm for different values of the noise characteristic time τ_D. In Fig. 3.3 (and Fig. 3.4) the error bars represent the maximum range of ISD variation.

In accordance with the analytical theory, no possibility to suppress the intrinsic noise has been found, although the ISD decreases with the decreasing of the noise correlation time τ_D.

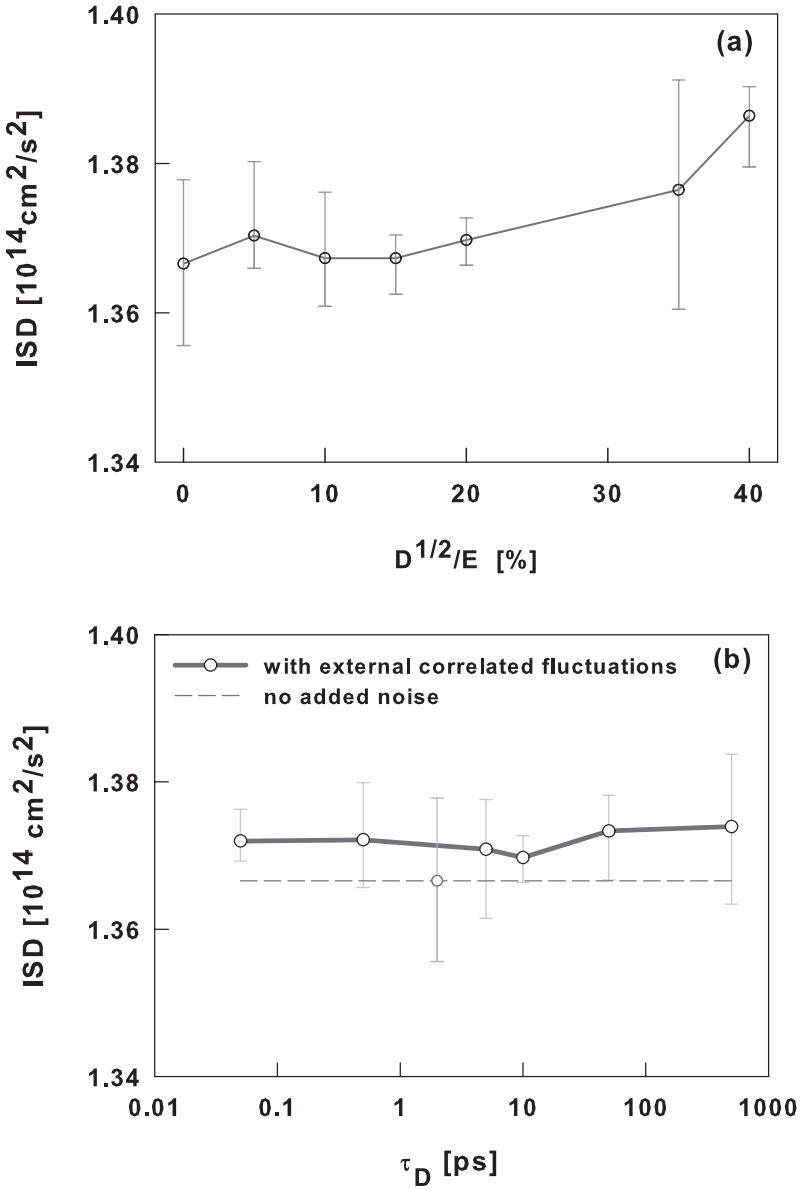

Figure 3.5: ISD of the velocity fluctuations as a function of: (a) the ratio between the noise amplitude $D^{1/2}$ and the deterministic component of the electric field E, obtained for E = 4 kV/cm and τ_D = 10 ps; (b) the noise correlation time τ_D, for E = 4 kV/cm and $D^{1/2}$ = 0.8 kV/cm.

Subsequently, we investigated the transport electron dynamics in the silicon MOS inversion layer, driven by a static electric field with an amplitude of E=4 kV/cm. This is because $d^2S(E_0)/dE^2$ is negative for field strengths lower than 5 kV/cm (see Fig.3.2).

In Fig. 3.5a we show the ISD obtained with the addition of a source of correlated noise, with a characteristic time of τ_D = 10 ps, as a function of the

ratio between the noise amplitude $D^{1/2}$ and the static electric field E.

The fact that the ISD, i.e. the variance of the velocity fluctuations, remains almost constant over the whole range of noise amplitude investigated, implies that if the noise is suppressed in a certain frequency range, it must be enhanced in another range in order to keep a constant value for the total power of the fluctuating signal. In this case, we obtain a noise redistribution, rather than a noise suppression.

For E = 4 kV/cm and a correlated noise with amplitude $D^{1/2}$ = 0.8 kV/cm (20% of the amplitude of the field), it remains almost constant in spite of the fact that the noise correlation time varies of about five order of magnitude.

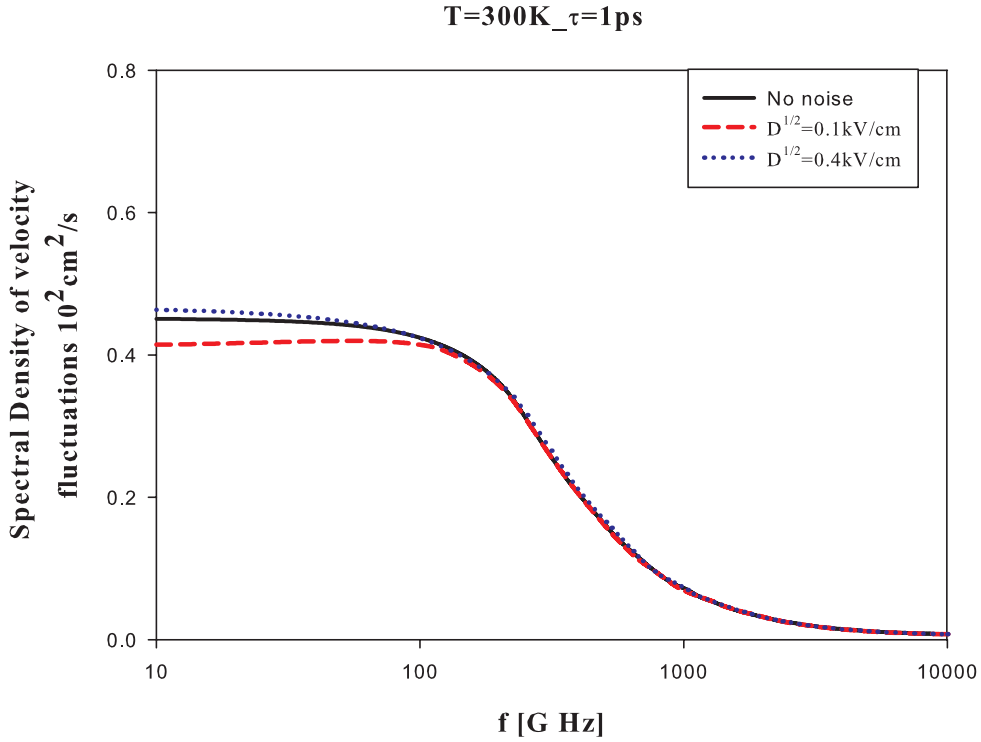

Figure 3.6: Spectral densities of velocity fluctuations obtained by a static electric field E= 1 kV/cm with a temperature of T=300K and the addition of a correlated source of noise with τ_D= 1ps and for two different values of the noise intensity D.

Since the results obtained in the presence of a static electric field of more than 2kV/cm showed no positive effects on the intrinsic noise of the system considered, we investigated the effect on the intrinsic noise caused by the addition of an external correlated noise source in a quasi-two-dimensional electron gas (2DEG) in a Silicon MOS inversion layer, driven by a constant

electric field of low intensity (E=1kV/cm), for different lattice temperatures.

Fig. 3.6 shows the spectral densities of the velocity fluctuations obtained by a static electric field E= 1 kV/cm with a temperature T=300K and the addition of a correlated source of noise with τ_D= 1ps, for two different values of the noise intensity $D^{1/2}$ (namely $D^{1/2}$ = 0.1 and 0.4kV/cm).

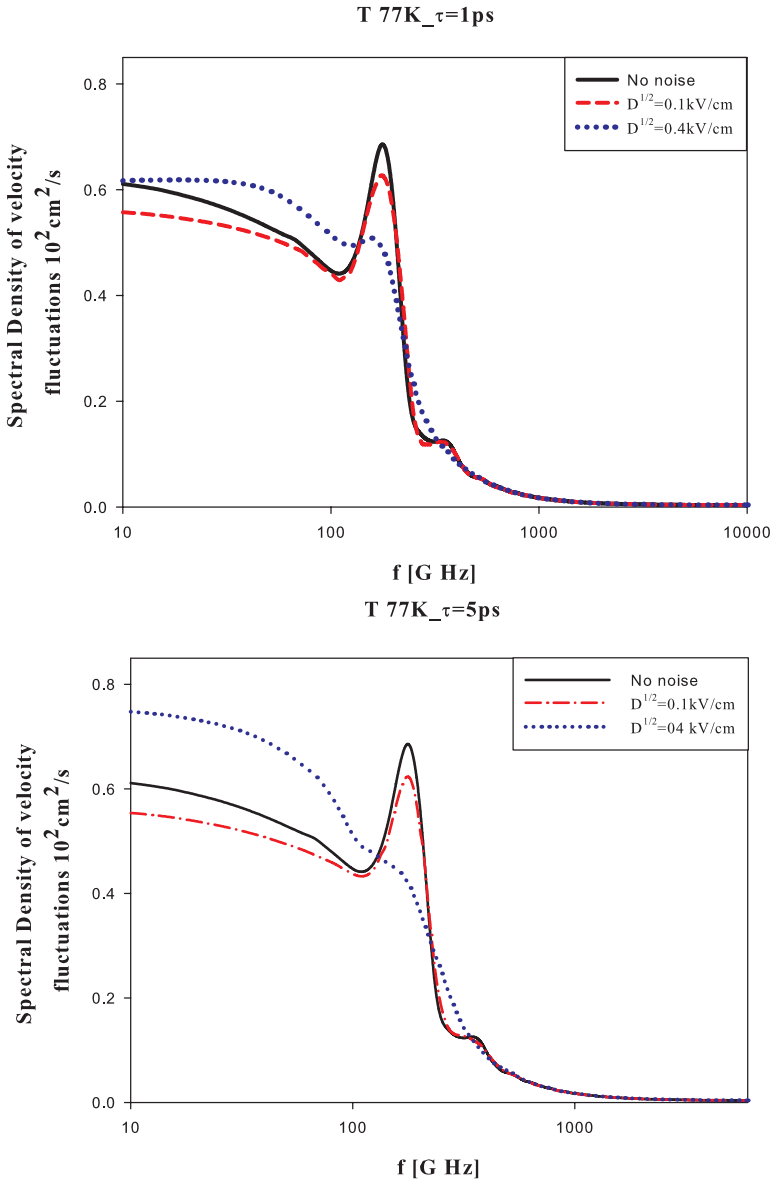

Figure 3.7: Spectral densities of velocity fluctuations obtained by a static electric field E= 1 kV/cm with a temperature of T=77K and the addition of a correlated source of noise with τ_D= 1ps and τ_D= 5ps, for two different values of the noise intensity D.

Fig. 3.7 shows the spectral densities of the velocity fluctuations obtained by a

static electric field E=1 kV/cm with a temperature of T=77K and the addition of a correlated source of noise with t_D= 1ps and t_D= 5ps, for two different values of the noise intensity $D^{1/2}$ (namely $D^{1/2}$ = 0.1 and 0.4kV/cm).

The effects of external noise are noticed at T=77K, while at T=330K there is only a small decrease in the low frequency region (see fig.3.6). Furthermore, the presence of noise reduces the height of the peak around 400 GHz at T=77K, in a way that depends on each value of intensity and correlation time studied. The low-frequency effect, on the other hand, depends heavily on both D and τ_D (see Fig.3.7).

The dependence of the intrinsic noise suppression effect on the amplitude and the correlation time of the external source of fluctuations have also been investigated by studying the integrated spectral density (ISD), i.e. the total noise power.

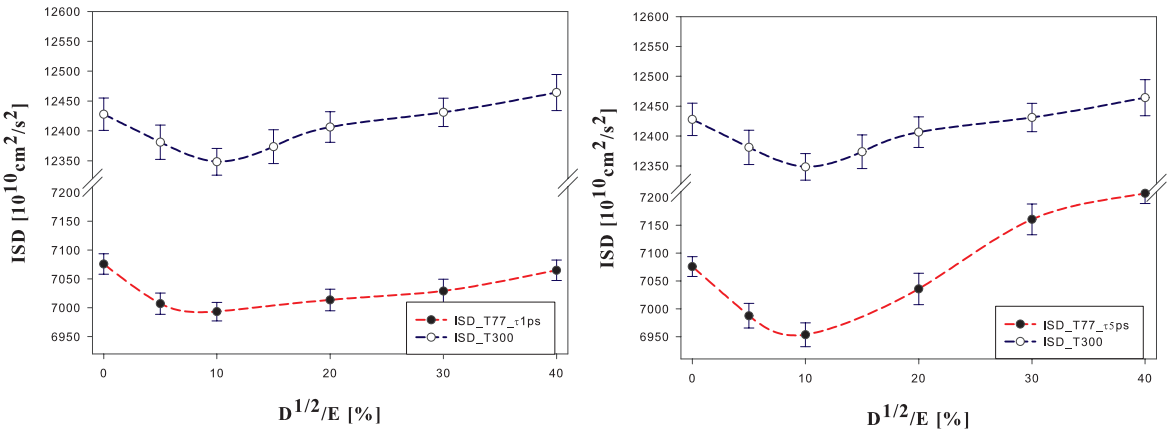

Figure 3.8: Integrated spectral density (ISD) obtained by a static electric field E=1kV/cm and the addition of a correlated source of noise with characteristic time of τ_D= 1ps and τ_D= 5ps for different values of the noise intensity D, at T=300 K and at T=77 K

In Fig. 3.8 we show the ISD obtained with the addition of a source of correlated noise, with characteristic times of τ_D = 1 ps and τ_D = 5 ps, as a function of the ratio between the noise amplitude $D^{1/2}$ and the static electric field E=1kV/cm, at T=300K and T=77K.

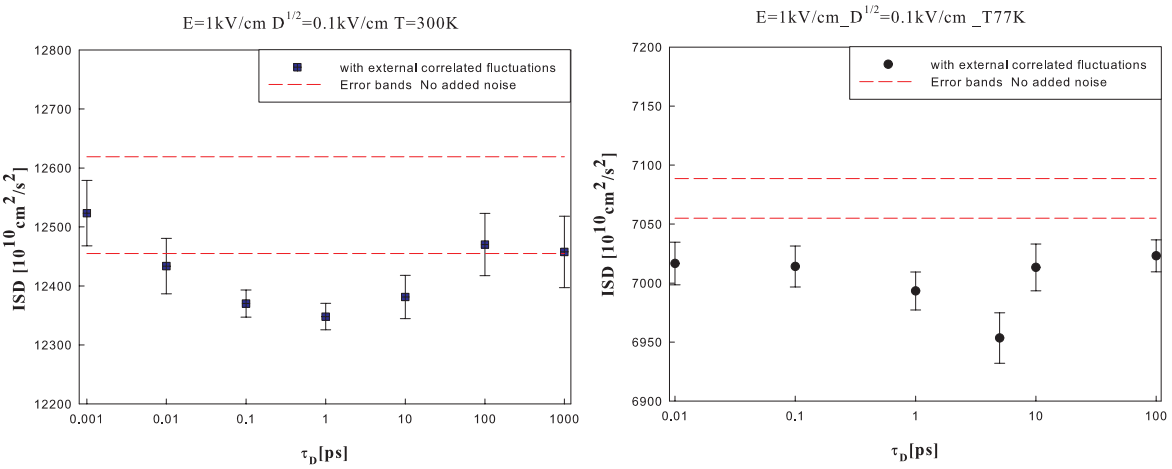

Figure 3.9: Integrated spectral density (ISD) obtained by a static electric field E=1kV/cm and the addition of a correlated source of noise with a noise intensity of D=0.1kV/cm for different values of the characteristic time, at T=300 K and at T=77 K

Fig. 3.9 shows the integral spectral density (ISD) of the velocity fluctuations obtained with E = 1 kV/cm and a source of correlated noise with $D^{1/2}$ = 1 kV/cm for different values of the noise characteristic time τ_D. The error bands (dotted lines) represent the maximum range of ISD in the absence of noise.

The ISD show a nonmonotonic behaviour. We observed that the total noise power decreases by up to 2% of the value obtained in the absence of external noise, especially at T=77K for τ_D = 5ps (see fig3.9), but only for noise amplitude by up to 15% of the amplitude of the deterministic electric field (see fig. 3.8).

Furthermore, an interesting aspect of non-monotonic behaviour by the ISD with the noise correlation time has been found. Further studies are needed to learn more about the interplay between the scattering processes' time scales and the noise correlation time in the possible suppression of the intrinsic noise.

Chapter 4

Hot-Electron Noise Features in Silicon Crystals operating under Periodic or Fluctuating Electric Fields

In this chapter, we initially focus on electron transport properties in n-silicon crystals embedded in high frequency alternating electric fields. The noise features of hot-carriers driven by the periodic electric field are compared with those obtained in the presence of a static field, with the aim of investigating the modifications of the electronic noise spectra induced by the frequency and the strength of the applied field.
Later we investigate noise-induced effects on the electron transport dynamics in the presence of two different kinds of external fluctuations: a dichotomous Markovian noise and a Gaussian correlated noise.

4.1 Noise features

The transport of the electrons in the Si bulk is simulated by using a single-particle Monte Carlo algorithm, which follows the standard procedure

described in chap.1.

The model for the conduction band of silicon and the parameters of the scattering mechanisms are the same as those described in chap.1.

4.1.1 Static electric field

Figure 4.1 illustrates the spectral density of electron velocity fluctuations as a function of the frequency, obtained by varying the amplitude of the static electric field E_0 in the range 2–20 kV/cm, at two different lattice temperatures, namely T = 77 K (panel a) and T = 300 K (panel b). When the free carriers inside the semiconductor crystal are driven by a static electric field, the shape of the spectral density of electron velocity fluctuations very much depends on the strength of the field applied. At T = 77 K, for field amplitudes equal to E_0 = 2 kV/cm and E_0 = 5 kV/cm, the shape of the spectral density is characterized by significantly higher values in the low-frequency region, a characteristic peak at an intermediate frequency of ~200 and ~400 GHz respectively, and a rapid drop for higher frequencies. For field amplitudes equal to 10, 15, and 20 kV/cm, the spectra are characterized by lower values in the low-frequency region and a broad peak at a frequency of ~800 GHz. The peak, which could be viewed as a "natural" transition frequency of the system between different valleys, is found at a frequency that increases with the intensity of the applied field E_0.

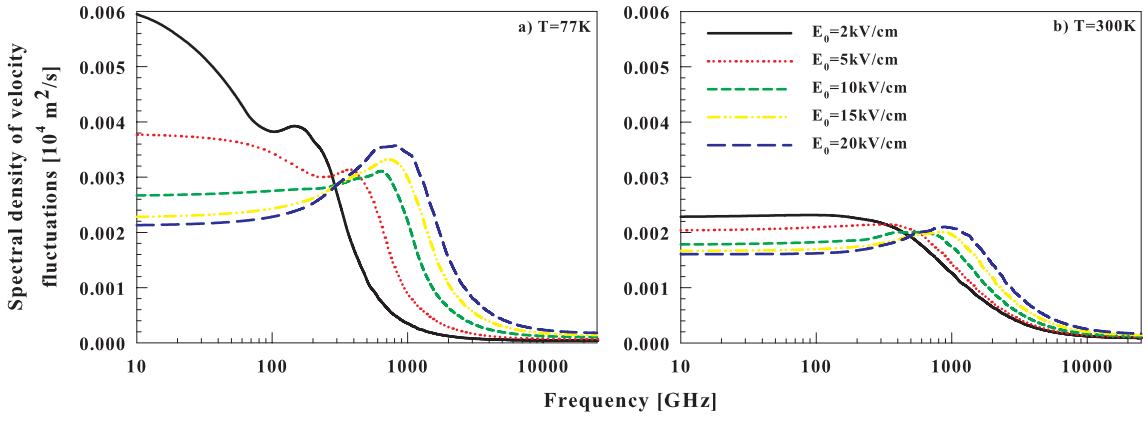

Figure 4.1. Spectral density of electron velocity fluctuations obtained for different strengths of the static electric field E_0 at two different lattice temperatures: (a) T = 77 K and (b) T = 300 K.

At T = 300 K (Fig. 4.1(b)), the spectral densities show a typical Lorentzian shape; the peaks are less pronounced and the enhancement at low frequencies is completely absent.

The total noise power, i.e. the integrated spectral density (ISD), is shown in Fig. 4.2 as a function of the amplitude of the applied static field. For the two lattice temperatures, the ISD shows an almost linear increase with E_0.

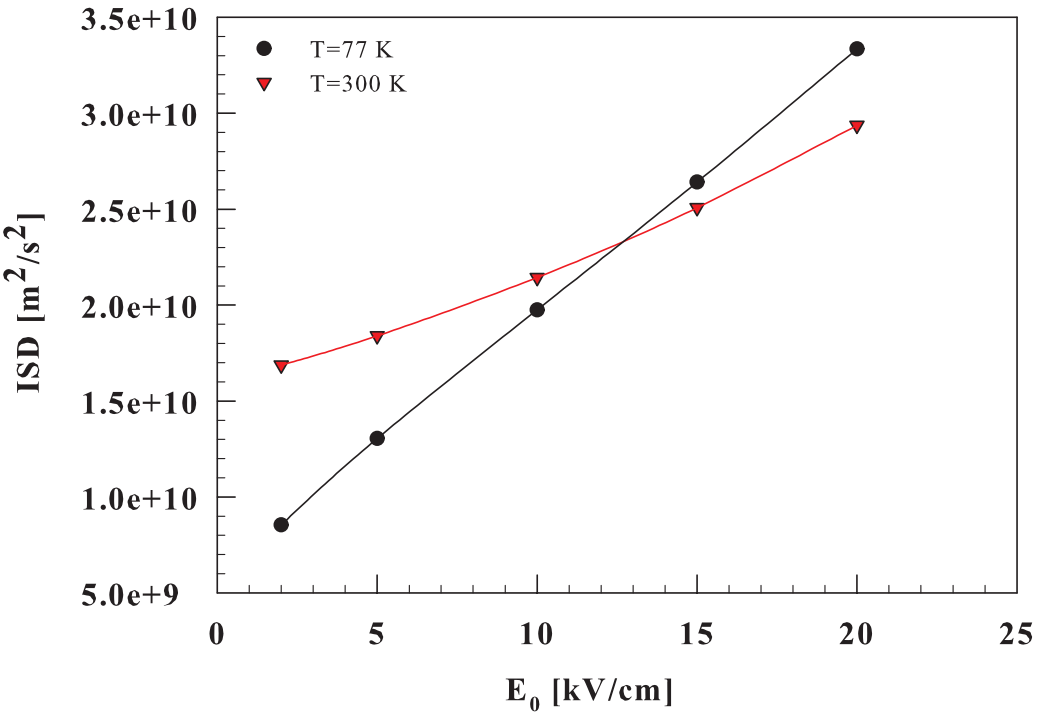

Figure 4.2: ISD of electron velocity fluctuations as a function of the amplitude of the applied static field *E0* at *T* = 77 K (black line) and *T* = 300 K (red line).

It is interesting to note that since the slope of the curve at T = 300 K is lower than that at T = 77 K, for field values greater than ~12 kV/cm the ISD at T = 300 K remains lower than the values computed at T = 77 K.

4.1.2 Oscillating electric field

In Fig. 4.3 we show the spectral density of electron velocity fluctuations obtained at T = 77 K, and field amplitude E in the range of 2 – 20 kV/cm at different frequencies, namely: (a) 100 GHz, (b) 200 GHz, (c) 500 GHz, and (d)

1THz.

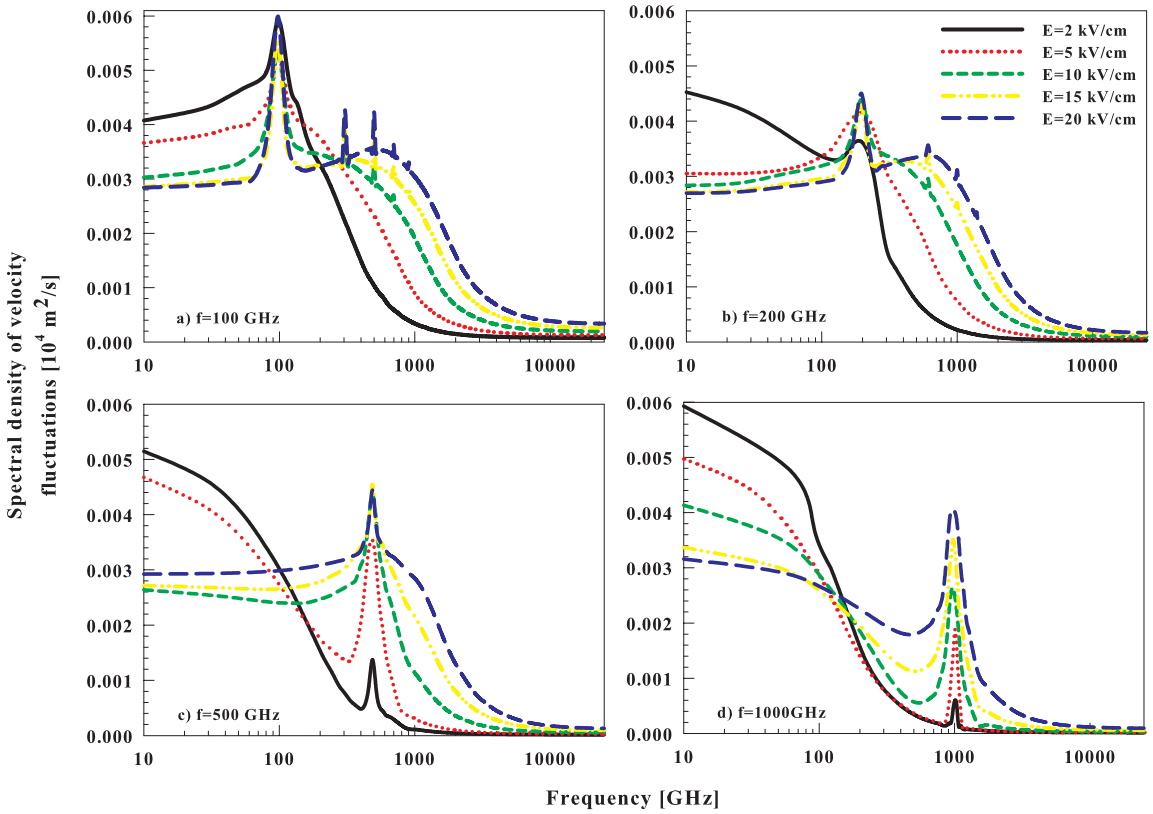

Figure 4.3: Spectral density of velocity fluctuations obtained in the presence of an external periodic electric field; T = 77 K and (a) f = 100 GHz, (b) f = 200 GHz, (c) f = 500 GHz, and (d) f = 1 THz.

For f=100 GHz, the spectra show the characteristic shape enriched by the presence of peaks at frequency f, and at its odd harmonics (up to the 11th for E = 20 kV/cm). In the low frequency range, the spectral density monotonically decreases with the increase in the electric field amplitude.

At f = 200 GHz, the spectra obtained at E = 2 kV/cm and E = 5 kV/cm show a significant enhancement in the low-frequency region and a more pronounced peak at frequency ν = 200 GHz. For stronger field amplitudes, the spectral density assumes the diffusion shape again. For f = 500 GHz and f=1THz, the peaks at the harmonic frequencies are not observed. Furthermore, an enhancement in the low-frequency region is found for E= 2 kV/cm, E = 5 kV/ cm at f = 500 GHz and for E = 10 kV/cm at f = 1 THz.

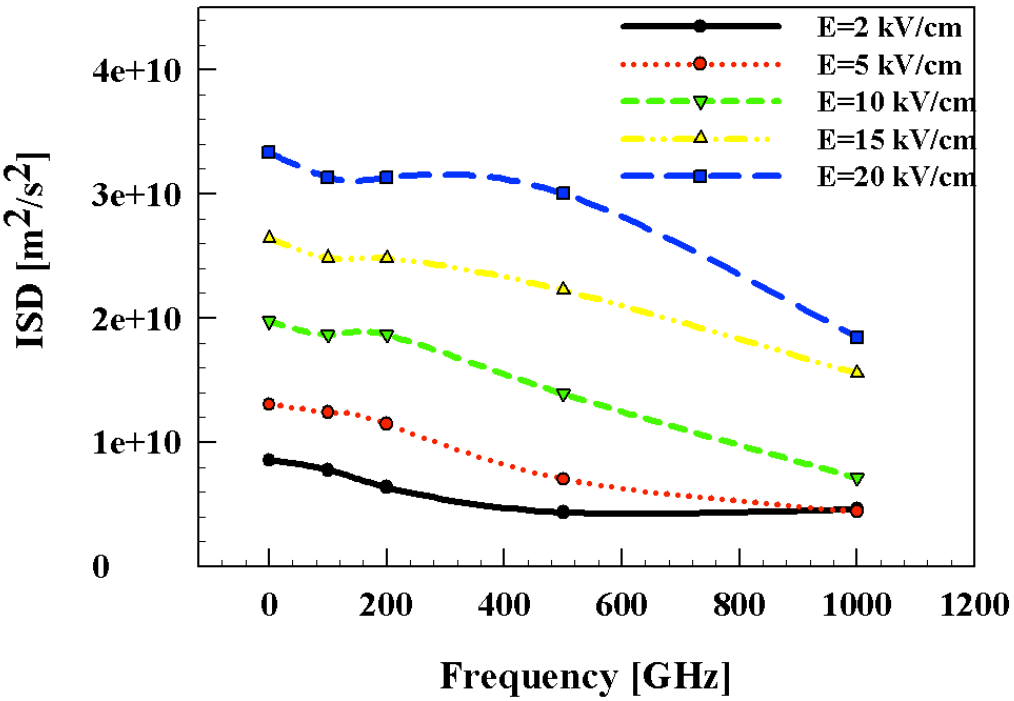

Figure 4.4: ISD of electron velocity fluctuations as a function of the frequency of the periodic field at different field amplitudes *E*.

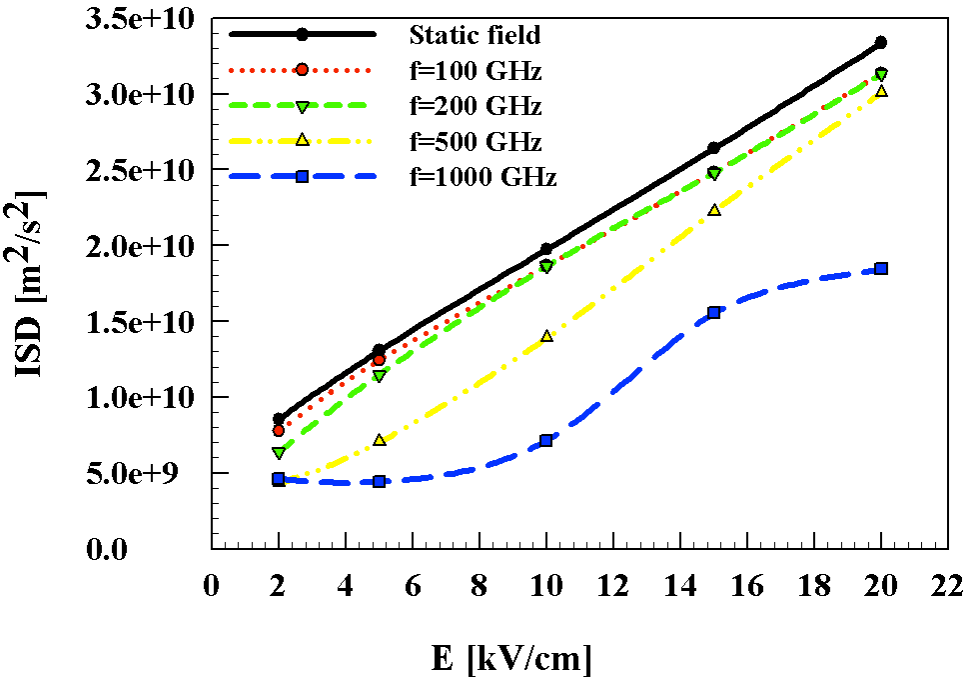

Figure 4.5: ISD of the electron velocity fluctuations as a function of the amplitude *E* of the periodic field at different values of frequency.

In Figs. 4.4 and 4.5 we show the ISD of the electron velocity fluctuations as a function of the frequency f of the driving electric field and as a function of the field amplitude E, respectively. The ISD obtained in the presence of an oscillating electric field is always lower than that computed in the static case for each amplitude of the applied field. It also monotonically decreases with the increase in the frequency of the driving field. For E = 2 kV/cm, it remains almost constant for frequencies of the periodic field in the range of 400 < f < 1000 GHz (see Fig. 4.4).

Furthermore, with the increase in the amplitude of the driving field, the ISDs up to f = 200 GHz show a linear increasing trend that remains close to the static one. Different increasing trends have been found in the case of f=500 GHz and f=1 THz. The ISD obtained at f = 1 THz, for E = 20 kV/cm, is reduced to about half of the value obtained in the static field case.

The noise spectra exhibit some peculiarities, which are very different from those obtained in the case of the static field. We noticed a significant reduction in the noise level for increasing frequencies of the driving field. This effect could be a consequence of the cooling of the distribution function, but further investigations are needed to clarify this result.

4.2 The noise-induced effects: numerical results and discussion

In this section we examine the noise-induced effects on the electron transport dynamics in low-doped n-type Si crystals operating under a high-frequency periodic electric field in the presence of two different kind of external fluctuations: a Gaussian correlated noise (see eq. 2.11) and a dichotomous Markovian noise (see eq.2.15)

The effects caused by the addition of an external noise source are investigated by studying the modifications in the correlation function of the electron velocity fluctuations and in its spectral density.

The spectral density of the electron velocity fluctuations has been studied by adopting a fluctuating periodic electric field with frequency f = 500 GHz.

The amplitude of this field has been chosen on the basis of a preliminary analysis of the variance of velocity fluctuations and the spectral density $S_0(E)$ at zero frequency, as a function of the amplitude of the oscillating field.

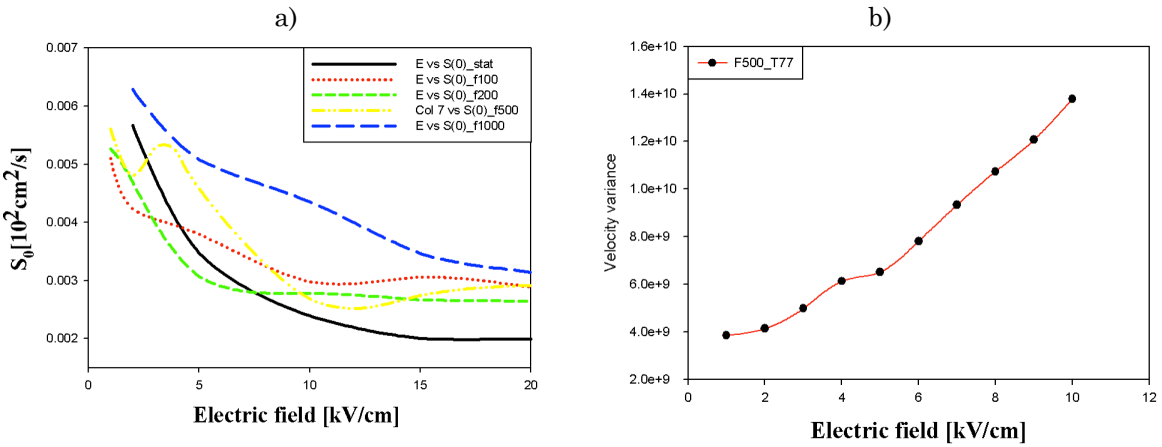

Figure 4.6: a) Spectral density of the velocity fluctuations at zero frequency (S_0) as a function of the electric field calculated by the Monte Carlo simulation at temperature T =77K. b) Variance of velocity fluctuations as a function of the electric field calculated at f=*500GhZ*

Following [6] and [9], the most favourable condition for obtaining a noise suppression effect in our system is atained when $d^2S_0(E)/dE^2$ is negative and the variance of velocity fluctuations reaches a maximum.

In figure 4.6, we can see which range of amplitudes of electric field verifies these conditions. We have chosen a driving electric field accordingly, with amplitude E_0 = 4 kV cm^{-1} and frequency f = 500 GHz.

In figure 4.7 we plot the correlation function of single particle velocity fluctuations obtained in the presence of (a) an external correlated noise, and (b) a dichotomous Markovian noise with amplitude $D^{1/2}$ = 0.4 kV/cm, for three different values of the noise correlation time t_D. We can see a decrease for all three different values of t_D.

In the absence of external noise, the features described in section 4.2 characterize the spectrum.

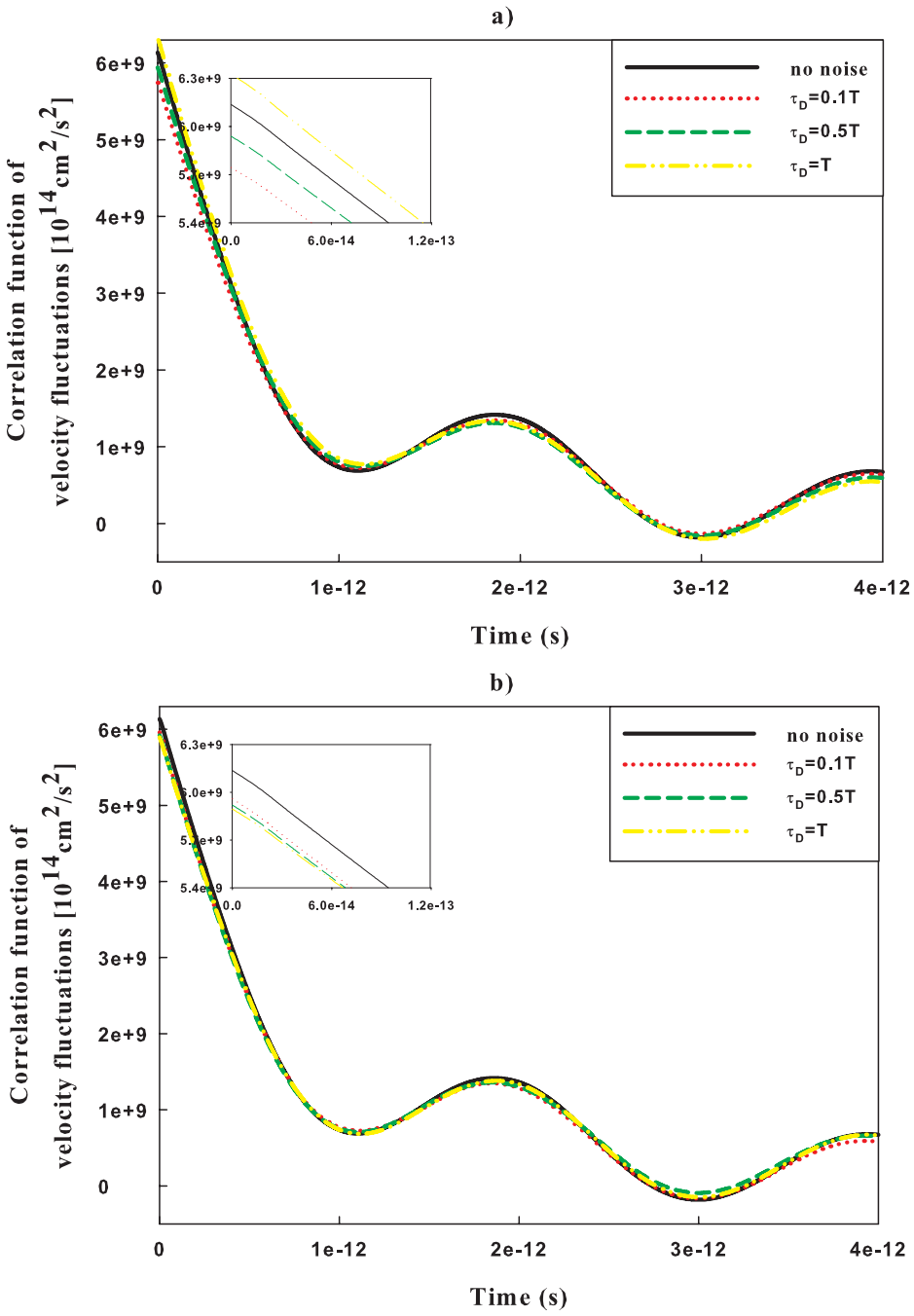

Figure 4.7 Correlation function of single particle velocity fluctuations obtained in the presence of (a) an external correlated noise, (b) a dichotomous Markovian noise, for three different values of the noise correlation time t_D. (E=4kV/cm T =77 K and f=500 GHz, $D^{1/2}$ = 0.4 kV/cm).

In figure 4.8 we show how the spectral density of electron velocity fluctuations is modified by the presence of a) a correlated noise, and (b) a dichotomous Markovian noise.

The addition of an external source of fluctuations to the driving electric field changes the spectrum and, in particular, the height of the peak around 500 GHz, in a way that depends on the correlation time.

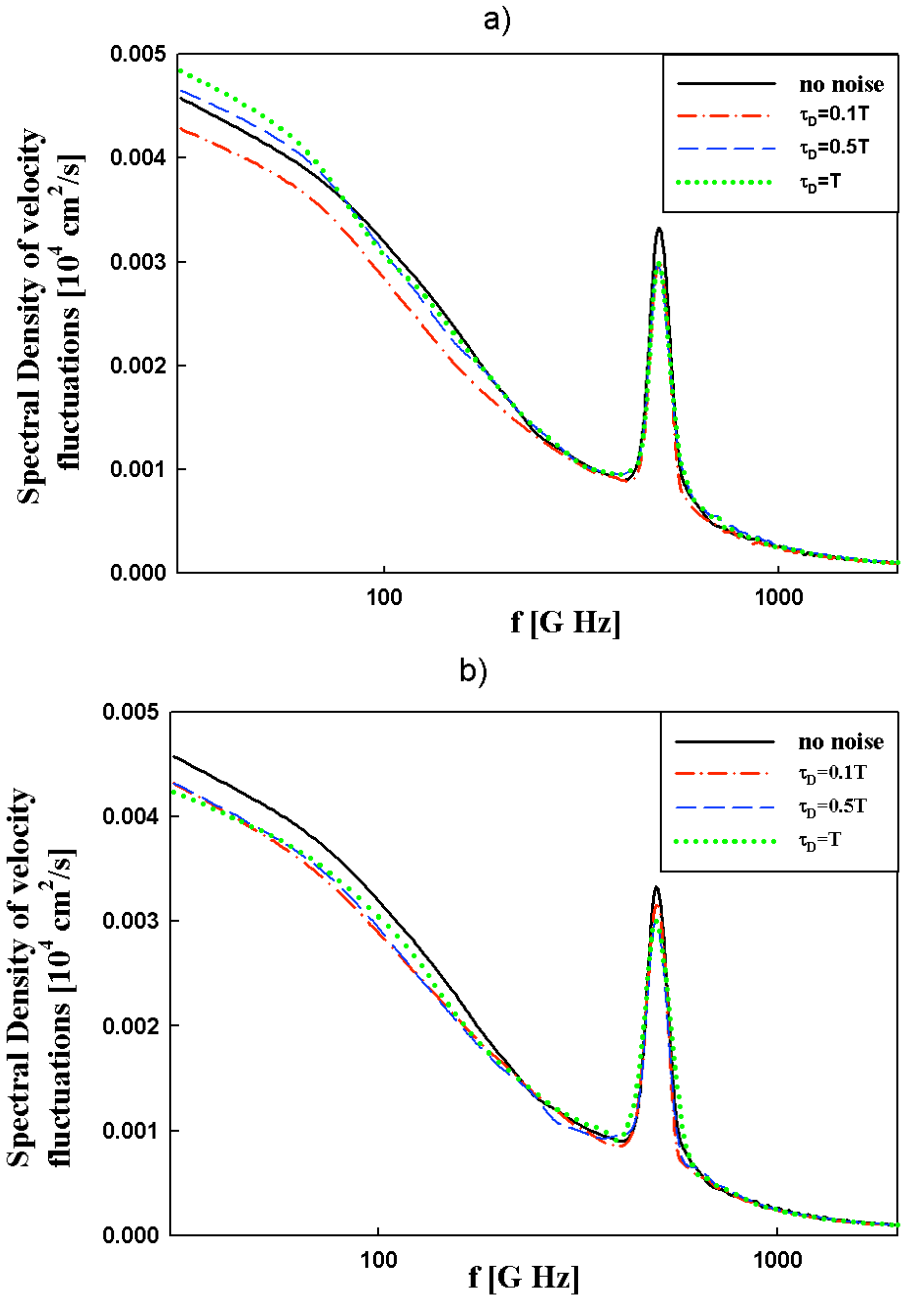

Figure 4.8: Spectral densities of single particle velocity fluctuations obtained in the presence of (a) an external correlated noise, (b) a dichotomous Markovian noise, for three different values of the noise correlation time t_D. (E=4kV/cm T =77 K and f=500 GHz, $D^{1/2}$ = 0.4 kV/cm).

The dependence of the intrinsic noise suppression effect on the amplitude and the correlation time of the external source of fluctuations has also been investigated by studying the integrated spectral density (ISD), i.e. the total noise power, as a function of the noise amplitude and the correlation time.

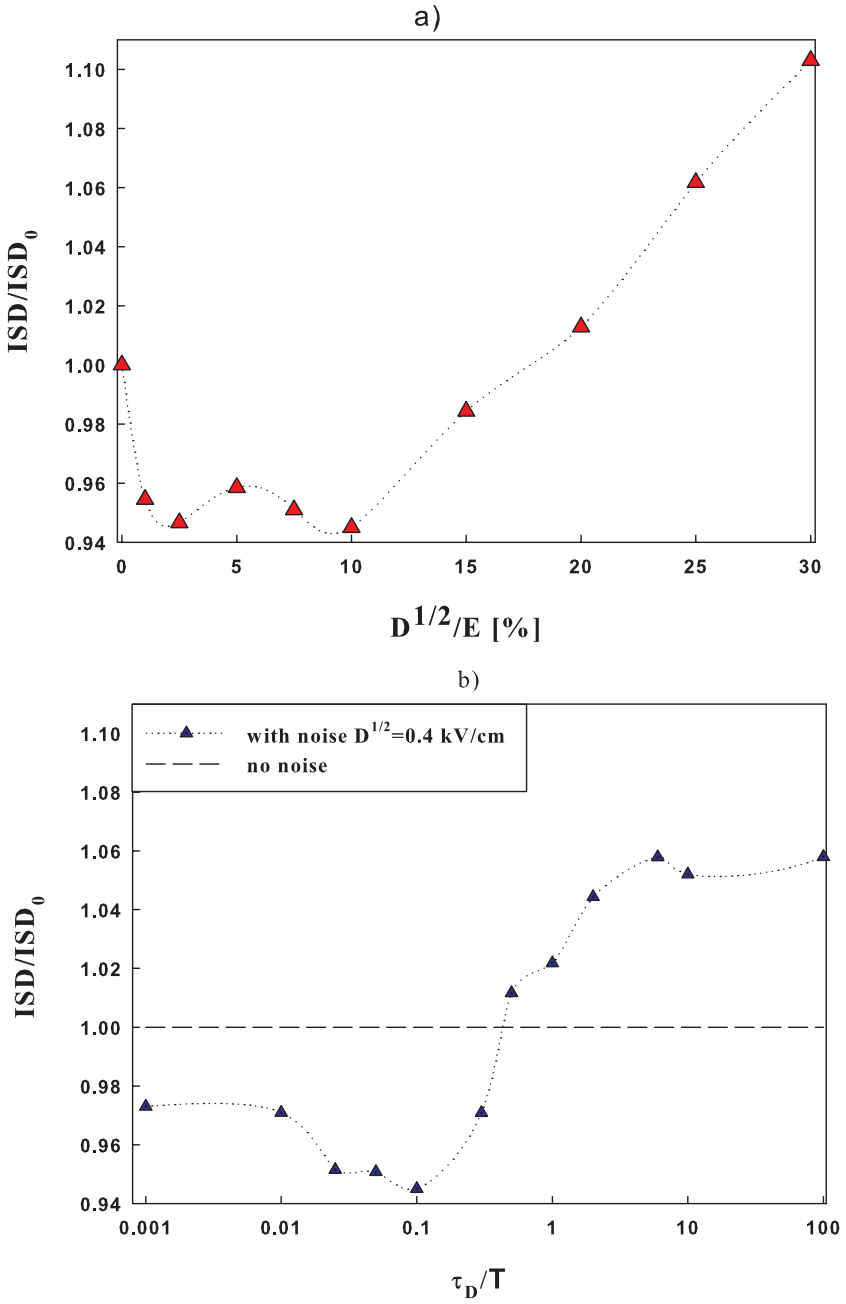

Figure 4.9 Integrated spectral density (ISD) of the electron velocity fluctuations as a function of (a) the values of the correlated noise amplitude $D^{1/2}$ (with a correlation time $\tau_D = 0.1T$) and (b) the values of the correlation time of the external source of noise, with amplitude $D^{1/2} = 0.4$ kV/cm .

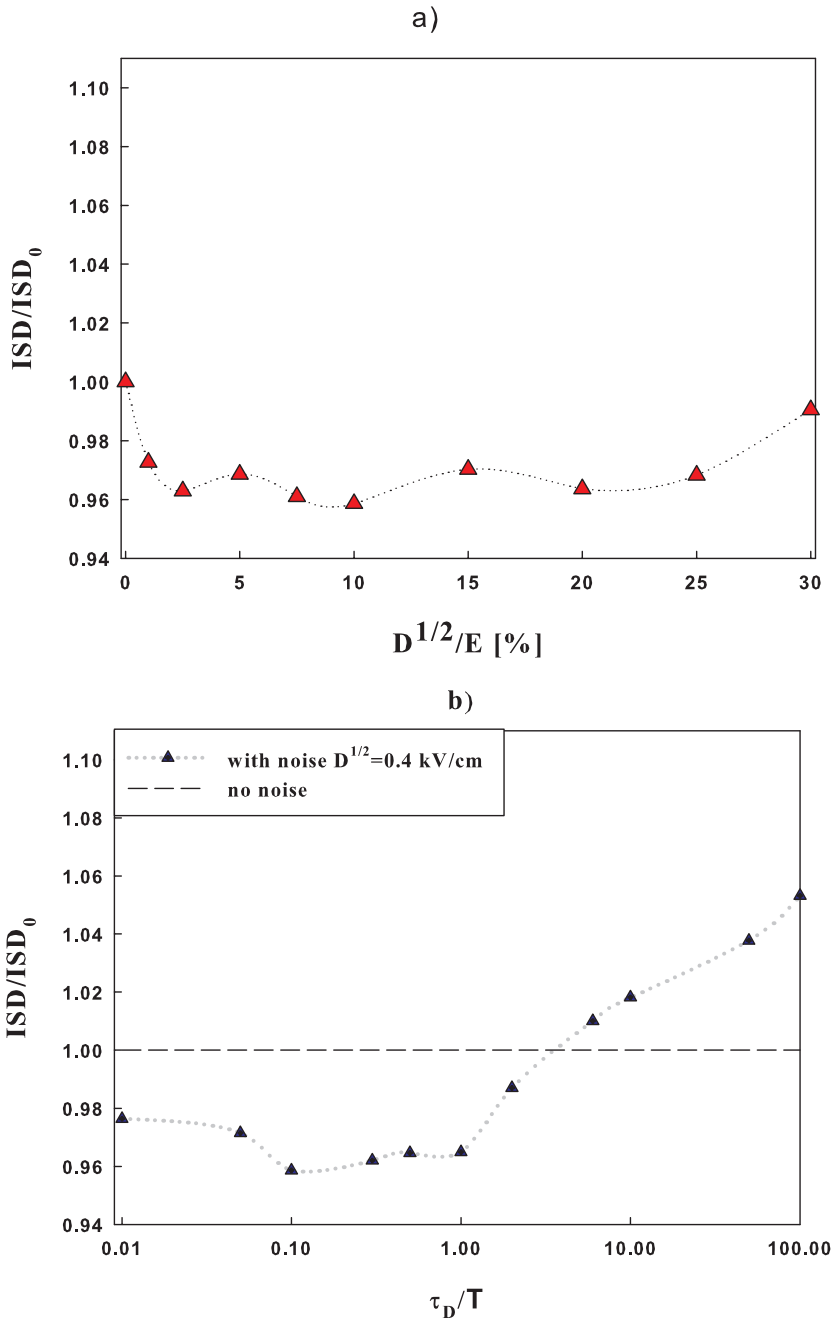

Figure 4.10 Integrated spectral density (ISD) of the electron velocity fluctuations as a function of (a) the values of the dichotomous Markovian noise amplitude $D^{1/2}$ (with a correlation time t_D = 0.1T) and (b) the values of the correlation time of the external source of noise, with amplitude $D^{1/2}$ = 0.4 kV/cm .

In figures 4.9 and 4.10, we show a reduction of the ISD in the presence of external noise. In particular, in the case of the addition of a Gaussian

correlated component to the deterministic field, the ISD as a function of the noise amplitude shows a nonmonotonic behaviour.

It can be observed that the total noise power decreases by up to 6% of the value obtained in the absence of external noise, but only for noise amplitude, by up to 10% of the amplitude of the deterministic oscillating electric field. The benefit is present only for values of a noise correlation time smaller than 0.5 T (where T is the field period).

The addition of a source of DM noise to the oscillating driving electric field can reduce the total noise power by up to 5%. We find this reduction in the whole range of amplitudes of the external fluctuations investigated (up to 30% of the amplitude of the deterministic oscillating electric field). Furthermore, this effect is present for values of the noise correlation time up to 10 T (where T is the field period). For longer noise correlation times, the total noise power increases compared with the case of deterministic driving fields.

Chapter 5

Monte Carlo Simulation of Spin Relaxation of Conduction Electrons in Silicon

In previous chapters, we have seen how noise can assume a control role in transport phenomena, which is particularly relevant in nano-scale systems and devices. Furthermore, externally added noise may also assume a control role in the spin relaxation process. In spin-based devices, the information stored in a system of polarized electron spins, must be transferred, as attached, to mobile carriers by applying an external electric field [91]-[94], [46, 95]. In order to avoid nonlinear response, applied voltages are very low. Since low voltages are more susceptible to background noise, in the design of spintronic devices it is essential to understand the influence of fluctuations of the electric field on the spin depolarization process.

In this chapter, we present the preliminary results obtained by using a semiclassical Monte Carlo (MC) approach to simulate both the electron transport and the spin dynamics. Spin relaxation is taken into account through the Elliot-Yafet mechanism [56, 57], which is dominant in-group IV materials. First, we validate the MC algorithm by comparing our numerical outcomes with those provided by the most recent theoretical models. Our results are in close agreement with the findings obtained from various analytical calculations. Furthermore, this chapter provides the experimental researcher

with an estimate of the spin lifetimes of drifting electrons in n-type Si crystals, at different temperatures and under different electron transport conditions.

5.1 Spin relaxation dynamics

In a silicon bulk, the Dyakonov-Perel spin relaxation mechanism is absent, due to its inversion symmetry, and under a non-degenerate regime, the spin depolarization process is mostly related to mechanisms in which electron spins have a small chance of flipping during each scattering. Spin-flip mechanisms can be classified within the Yafet and Elliott processes [56, 57]. The Yafet process involves spin-dependent interactions, whereas the states are viewed as pure spin states. The Elliott processes, on the other hand, are governed by spin mixing in the electron states of the conduction band, due to the crystal spin-orbit coupling, whereas the interaction is spin independent. In fact, in the presence of spin-orbit interactions, the electronic Bloch states are given by a mixture of pure spin-up $|\uparrow\rangle$ and spin-down $|\downarrow\rangle$ states [56, 57]:

$$|\mathbf{k},\Uparrow\rangle = [a_k|\uparrow\rangle + b_k|\downarrow\rangle\,]e^{i\boldsymbol{k}\cdot\boldsymbol{r}}$$
$$|\mathbf{k},\Downarrow\rangle = [a^*_{-k}|\downarrow\rangle + b^*_{-k}|\uparrow\rangle\,]e^{i\boldsymbol{k}\cdot\boldsymbol{r}} \qquad (5.1)$$

with the lattice momentum **k,** effective spins $\Uparrow$, $\Downarrow$ and the spin-mixing parameter $|b_k|^2$. Both states have the same energy. For conduction electrons in silicon, spin-flip scattering is described by a matrix element that depends on the initial and final state wave vectors, as well as on the spin orientation, which has the form

$$\langle \mathbf{k_2},\Downarrow|\boldsymbol{H_{SF}}\,|\mathbf{k_1},\Uparrow\rangle \qquad (5.2)$$

where H_{SF} is a given spin-flip mechanism. The Elliot-Yafet spin lifetime τ_s can be related to the momentum relaxation time τ_m by the following expression [56, 96, 97]:

$$\tau_S = \frac{\tau_m}{4\langle b^2\rangle} \qquad (5.3)$$

where $\langle b^2 \rangle$ is the Fermi surface average of the spin-mixing parameter. However, this relationship is not very accurate in silicon. In fact, it has been pointed out that:

(i) the spin-mixing parameter $|b_k|^2$ varies in a broad range of values, depending on the value of the momentum **k** [96];

(ii) the scattering mechanisms dominating the relaxation of the momentum are different from those leading to spin relaxation [98,99].

The correct way to elucidate the spin relaxation mechanisms is by calculating the explicit form of the spin-flip electron-phonon matrix elements for the conduction states. Different theoretical approaches have addressed the calculation of both the spin mixing probabilities and the matrix element expressions for all the phonon-induced spin-flip transitions in the conduction band. These include, for example, the pseudopotential model reproducing spin-orbit splittings of the relevant electronic states [98, 100], the group theory, the k•p perturbation method, the rigid-ion model [99], the parameter-free first-principles method and the density fuctional perturbation theory [101], the adiabatic band charge models and the tight-binding models [102]. Starting from the detailed knowledge of a specific electron distribution, they calculate the relaxation rate τ_i for each different scattering mechanism. If several independent mechanisms of depolarization are present, the total spin relaxation time τ_s can be calculated by

$$\frac{1}{\tau_S} = \sum_i \frac{1}{\tau_i} \tag{5.4}$$

Short relaxation times are very important, while the longer ones can be neglected [103]. The approach we use here is different. Our MC code incorporates the electron spin dynamics by taking into account the spin mixing probabilities and the phonon-assisted spin flip transitions. We consider that the rates of transitions from the $|\Uparrow\rangle$ to the $|\Downarrow\rangle$ states are proportional to the square of the matrix elements of electron-lattice interaction, which causes a spin flip [56]. In particular, unlike the seminal work of Yafet [57], we take into account both intra and intervalley scattering. The spin mixing probability is of the order of 10^{-6}, and depends on the value of **k** [98, 100]. In particular, more

energetic electrons strongly drive the average spin relaxation. In our simplified model, we only consider the following for spin-flipping

- the intravalley acoustic phonons and
- all six phonon modes of the intervalley f-processes. Spin-flipping due to g- processes can be neglected because its contribution is not significant in the temperature range considered (60<T<300 K) (see Fig. 8 in Ref. [99]).

More details and the explicit calculation of the spin-flip matrix elements utilized in our code can be found in Refs. [98, 99]. The dependence of spin relaxation times on temperature and/or electric field amplitude has been investigated by simulating the dynamics of 5×10^3 electrons, initially polarized (P = 1) along the x-axis of the crystal at the injection plane. We calculate the polarization P as a function of time by averaging over the ensemble of electrons. The spin lifetime τ_s corresponds to the time necessary to achieve a reduction of the initial spin polarization by a factor of 1/e.

5.2 Results and discussion [104]

First, we calculated the contribution of acoustic-AC and optical-OP phonon scattering to the spin relaxation process separately, in the absence of an applied electric field. The spin relaxation time τ_s as a function of the crystal temperature is shown in Figure 5.1, where the contributions of AC-phonon (upper panel) or OP-phonon (lower panel) scattering mechanisms are considered. In each panel, our numerical findings are compared with the results provided by recent theoretical approaches. The agreement with the analytical trends is satisfactory in the whole range of lattice temperatures investigated. Furthermore, a comparison between the acoustic and optical phonon contribution to spin relaxation shows that AC phonon scattering is dominant in the low temperature range (T<200 K), while OP phonon assisted spin-flip transitions can no longer be neglected at higher temperatures. This is consistent with the fact that at smaller energies (lower temperatures) long-wavelength acoustic phonon modes are more populated, whereas the growth of the phonon population with temperature for optical modes is faster than for

acoustic modes.

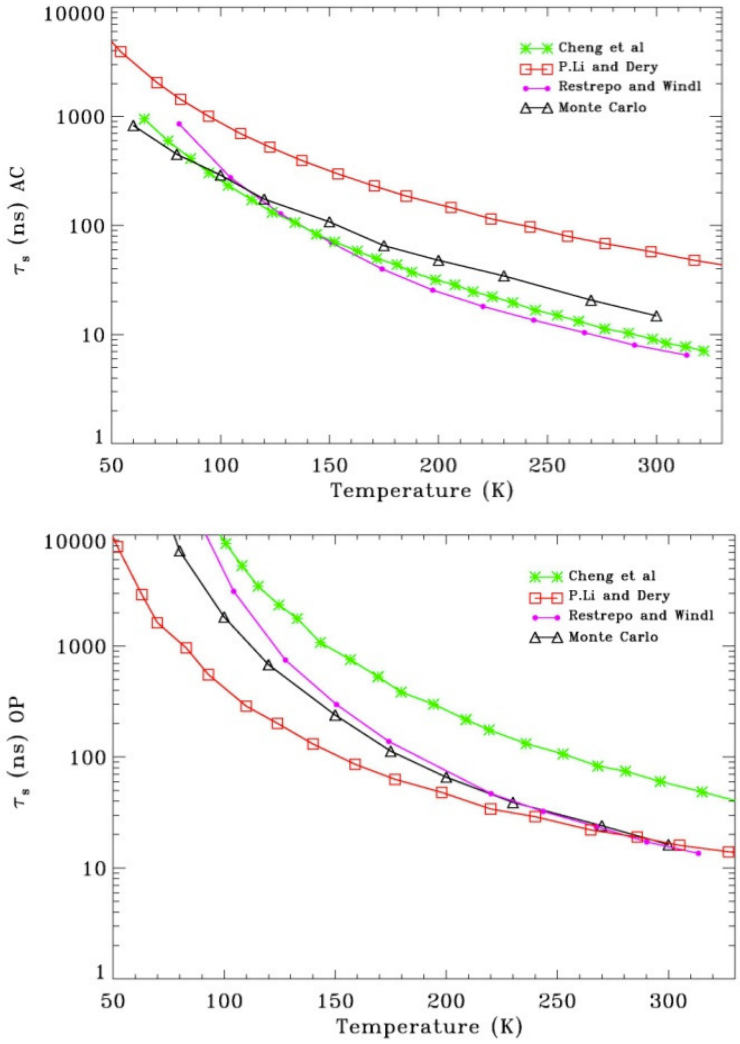

Figure 5.1. Comparison between the MC-computed contributions to the spin relaxation process of acoustic-AC (upper panel) and optical-OP (lower panel) phonon scattering, and the results from recent theoretical approaches, as a function of temperature.

In Fig. 5.2 the total electron spin lifetime computed in our simulations is compared with recent theoretical and analytical findings, as a function of the temperature. Although our MC code still does not take into account the scattering of electrons with g-phonons and the interactions with impurities, and uses approximated relations for the spin-flip rates, the close agreement with the analytical theories, in the absence of applied electric fields, strengthens the reliability of our MC algorithm.

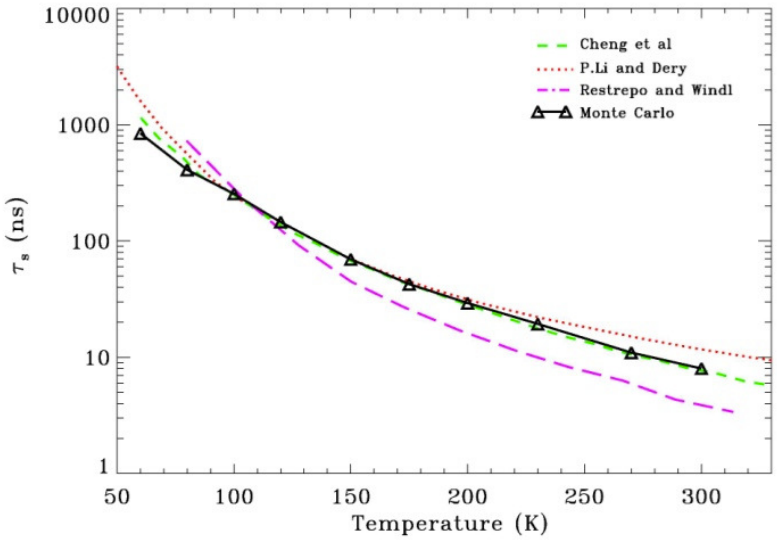

Figure 5.2. Comparison between our MC numerical total spin lifetime and the results from recent theoretical approaches, as a function of the temperature.

Figure 5.3 shows the spin lifetimes calculated in the presence of an electric field applied along the x- axis of the crystal, at three different temperatures, namely T=90, 120 and 300 K.

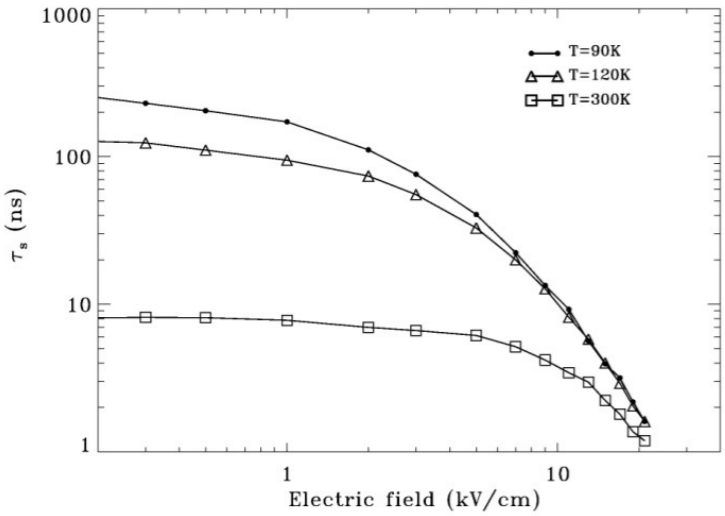

Figure 5.3: Electron spin lifetime as a function of the applied electric field at three different values of the temperature.

The presence of the driving electric field significantly affects the electron momentum distribution, which deviates from the equilibrium condition even at

low temperatures. This results in an enhancement of intervalley scattering and explains the rapid drop of spin lifetimes observed at electric fields higher than 3 kV/cm. At room temperature, where no experimental data are yet available, our calculation predicts spin lifetimes of the order of 8 ns up to field amplitudes ~ 5 kV/cm. When the electric field amplitude is maximum (E= 20 kV/cm), the effect of the temperature becomes almost negligible; all the three curves collapse and the spin relaxation times take on values between 1 and 2 ns.

5.2 Future prospects

The understanding of spin-related properties and spin transport in Si and related compounds is important for solid state physics, and possible applications of these materials in spintronics. In fact, in order to make spintronics a viable prospective technology, we need to find out the best conditions to achieve long spin relaxation times (or spin diffusion lengths) in semiconductor materials.

In the future we will focus our attention on the calculation of the modifications of the spin depolarization length caused by the addition of an external source of correlated noise in Si bulk semiconductors, for different values of the static field strength, noise amplitude and correlation time.

Conclusions

Noise in semiconductor devices has a significant impact on the performance of circuits. The capability to measure and characterize semiconductor device noise is a fundamental requirement for design. Noise characterization is also important to monitor semiconductor processes quality. Furthermore, in the design of spintronic devices it is essential to understand the influence of fluctuations in the electric field on the spin depolarization process. Previous detailed studies of the electron transport dynamics in a GaAs bulk, working under static or cyclostationary conditions, have revealed that, under specific conditions, the addition of a fluctuating component to the driving field can reduce the total noise power. Various studies of the electron spin relaxation process in GaAs bulks, at nitrogen temperature, have shown that a random contribution added to the static electric field can affect the spin decoherence length [49, 50].

On the other hand, to the best of our knowledge, no conditions have been found to suppress the electronic intrinsic noise in silicon bulk. Recently, electrical injection of spin polarization in n-type and p-type silicon up to room-temperature have been experimentally carried out [51-53], but a comprehensive investigation into the influence of transport conditions on the spin depolarization process in silicon structures, in a wide range of values of temperature and amplitude of external fields, is still missing.

In the wake of these findings, this thesis has focused on:

- the investigation of the effects of the addition of an external source of noise on the carrier velocity fluctuations in Si semiconductor bulk and 2D (Si MOS inversion layer);
- the development of a comprehensive theoretical framework concerning the influence of transport conditions on the spin depolarization process in

silicon structures, at a wide range of temperatures, doping concentrations and amplitudes of external fields

In our studies, we used a numerical code Monte Carlo to simulate the transport and spin dynamics of the electrons in homogeneous semiconductors, in the presence of static periodic or fluctuating electric fields. All results were obtained in Si with a free electron concentration 10^{13} cm^{-3} (nondegenerate low-doped n-type). We assumed that all donors are ionized and that the free electron concentration is equal to the doping concentration.

Initially we investigated the effect on the intrinsic noise caused by the addition of external correlated fluctuations in a silicon MOS inversion layer, driven by a static electric field, for different values of both noise amplitude and correlation time. Our numerical results showed that if the amplitude of the driving field is E = 10 kV/cm, the spectrum of velocity fluctuations only changes in an appreciable way in the low-frequency region (f < 500 GHz). Furthermore, in the range of the amplitudes and correlation times of the external noise investigated, the transport dynamics of the Q2DEG do not received any benefit, in terms of a total noise power reduction. This also happens when the noise characteristic time is varied. If, on the other hand, the amplitude of the applied field is reduced to E = 4 kV/cm, in the presence of correlated noise, the variance of velocity fluctuations remains almost constant. This result implies that if the noise is suppressed in a certain frequency range, it must be enhanced in another range in order to keep a constant value of the total power of the fluctuating signal. Furthermore, the performances of semiconductor-based devices, working on a noisy environment, were not significantly affected. Since the results obtained in the presence of a static electric field greater than 2kV/cm showed no positive effects on the intrinsic noise of the system considered, we investigated the effect on the intrinsic noise caused by the addition of an external correlated noise source to a constant electric field of low intensity (E=1kV/cm), for different lattice temperatures T=300K and T=77K. The positive effects of external noise are observed at T=77K, while at T=300K there is only a small decrease in the low frequency region. Furthermore, the presence of noise reduces the height of the peak around 400 GHz to T=77K, in a way that depends on the intensity and correlation time of

the none.. The ISD obtained with the addition of a source of correlated noise, at T=300K and T=77K, shows nonmonotonic behaviour as a function of the none amplitude. In particular we observed that the total noise power decreases by up to 2% of the value obtained in the absence of external noise, especially at T=77K for τ_D = 5ps, but only for noise amplitude by up to 15% of the amplitude of the deterministic electric field.

In the second part of the thesis, we studied the hot-carrier noise in n-type Si crystals operating under high-frequency periodic electric fields. The noise properties are investigated by computing the spectral density of the electron velocity fluctuations and the total noise power, for different values of the intensity and frequency of the driving field. The noise features of hot-carriers driven by the periodic electric field are compared with those obtained in the presence of a static field, with the aim of investigating the modifications of the electronic noise spectra induced by the frequency and the strength of the applied field. We found a considerable reduction in the noise level for increasing frequencies of the driving field. This effect could be a consequence of the cooling of the distribution function, but further investigations are needed to clarify this result. Future work will be focused on a complete understanding and physical interpretation of the electronic noise features observed in Si devices driven by periodic electric fields, with the aim of obtaining relevant information for harmonic extraction purposes.

Later we investigated the noise-induced effects on the electron transport dynamics in low-doped n-type Si crystals operating under a high-frequency periodic electric field, in the presence of two different kinds of external fluctuations: a dichotomous Markovian noise and a Gaussian correlated noise. The effects caused by the addition of an external noise source are investigated by studying the modifications in the correlation function of the electron velocity fluctuations and in its spectral density. The spectral density of the electron velocity fluctuations was studied by adopting a fluctuating periodic electric field with frequency f = 500 GHz.

The amplitude of this field was chosen on the basis of a preliminary analysis of the variance of velocity fluctuations and the spectral density $S_0(E)$ at zero frequency, as a function of the amplitude of the oscillating field.

In the presence of an externalsource of noise we observed a reduction of the ISD. In particular:

- in the case of the addition of a Gaussian correlated component to the deterministic field, the ISD as a function of the noise amplitude shows a nonmonotonic behaviour. We observed that the total noise power decreases by up to 6% of the value obtained in the absence of external noise, but only for noise amplitude of up to 10% of the amplitude of the deterministic oscillating electric field. The benefit is present only for values of the noise correlation time smaller than 0.5T (where T is the field period).
- the addition of a source of DM noise to the oscillating driving electric field can reduce the total noise power by up to 5%. We find this reduction in the whole range of amplitudes of the external fluctuations investigated (up to 30% of the amplitude of the deterministic oscillating electric field). Furthermore, this effect is present for values of the noise correlation time up to 10T (where T is the field period). For longer noise correlation times, the total noise power increases in relation to the case of deterministic driving fields.

Finally, in order to study the influence of fluctuations of the electric field on spin relaxation process in the future, we have developed a comprehensive theoretical framework concerning the influence of transport conditions on the spin depolarization process in silicon structures, by estimating both the spin lifetimes and the depolarization lengths as a function of the values of lattice temperature, electric field amplitude and doping density. In this thesis, we have given the preliminary results of the MC calculations of the spin lifetime for conduction electrons drifting in a silicon bulk. The electron spin total lifetime, computed in our simulations, has been compared, as a function of the temperature, with recent theoretical and analytical findings, showing that our numerical findings are in agreement with the results obtained by using different theoretical approaches. Furthermore, we also studied how spin lifetimes change in a wide range of temperature and electric field amplitudes. Our findings show that the presence of the driving electric field significantly affects the electron momentum distribution that deviates from the equilibrium condition even at low temperatures.

This fact is responsible for an enhancement of intervalley scattering and explains the rapid drop of spin lifetimes observed at electric fields higher than 3 kV/cm. At room temperature, where up today no experimental data are yet available, our calculation predicts spin lifetimes of the order of 8 ns up to field amplitudes ~ 5 kV/cm. When the electric field amplitude is high (E= 20 kV/cm), the effect of the temperature becomes nearly negligible; all the three curves collapse and the spin relaxation times take values ranging between 1 and 2 ns. From this point of view, our Monte Carlo simulations can guide experimental studies and be very useful in designing efficient silicon based spintronic-devices.

The future of this research will involve both the extension of the results obtained in heterostructures and nanostructures, and the study of the modifications of the spin depolarization length caused by the addition of an external source of correlated noise in Si bulk semiconductors, for different values of the static field strength, noise amplitude and correlation time.

Furthermore, our investigation of the effects produced by an external source of noise on the carrier velocity fluctuations and on the spin dynamics in semiconductors will be continued by using different sources of noise, i.e. Lévy noise and colored noise.

Bibliography

[1] Carlo Jacoboni and Lino Reggiani, "*The Monte Carlo method for the solution of charge transport in semiconductors with applications to covalent materials",* Reviews of Modern Physics, Vol. 55, No. 3, July 1983

[2] W. Shockley, "*Hot electrons in germanium and Ohm's law"*, Bell Syst. Tech. J. 30, 990 (1951).

[3] Marchuk, G. I., G. A. Mikhailov, M. A. Nazaraliev, R. A. Dar- binjan, B. A. Kargin, and B. S. Elepov, "*The Monte Carlo Methods in Atmospheric Optics*", Vol. 12 of Springer Series in Optical Sciences (Springer, Berlin), 1980

[4] R. Brunetti, C. Jacoboni, *"Analysis of the stationary and transient autocorrelation function in semiconductors",* Phys. Rev. B **29**, 5739 (1984)

[5] L. Varani, L. Reggiani, T. Kuhn, T. Gonzalez, D. Pardo, "*Microscopic simulation of electronic noise in semiconductor materials and devices"***,** IEEE Trans. Electr. Dev. 41, 1916 (1994).

[6] J.-P. Nougier, "*Fluctuations and noise of hot carriers in semiconductor materials and devices",* IEEE Trans. Electron Dev. 41, 2034 (1994).

[7] L. Reggiani, P. Golinelli, L. Varani, T. Gonzalez, D. Pardo, E. Starikov, P. Shiktorov, V. Gruzinskis, "*Monte Carlo analysis of electronic noise in semiconductor materials and devices*", Microelectronics Journal 28, 183 (1997).

[8] P. Shiktorov, E. Starikov, V. Gruzinskis, S. Pérez, T. Gonzalez, L. Reggiani, L. Varani, J. C. Vaissiere, "*Upconversion of partition noise in semiconductors operating under periodic large-signal conditions*", Phys. Rev. B 67, 165201 (2003).

[9] P. Shiktorov, E. Starikov, V. Gruzinskis, M. Zarcone, D. Persano Adorno, G. Ferrante, L. Reggiani, L. Varani and J.C. Vaissière, "*Monte Carlo Analysis of the Efficiency of Tera-Hertz Harmonic Generation in Semiconductor Nitrides"*, Physica Status Solidi A 190, 271 (2002).

[10] J.F. Millithaler, L. Reggiani, J. Pousset, L. Varani, C. Palermo, J. Mateos, T. Gonzalez, S. Pérez and D. Pardo, "*Plasmonic noise in nanometric semiconductor layers"*, J. Stat. Mech. Theor. Exp. P02030, (2009).

[11] S. Pérez and T. Gonzalez, "*Monte Carlo analysis of voltage noise in sub-micrometre semiconductor structures under large-signal regime*", Semiconductor Sci. Technol 17, 696 (2002).

[12] D. Pardo, J. Grajal, S. Pérez, B Menc´ıa, J Mateos and T Gonza´lez, "*Analysis of noise spectra in GaAs and GaN Schottky barrier diodes Semiconductor*", Sci. Technol 26, 055023 (2011).

[13] T. Gonzalez, S. Pérez, E. Starikov, P. Shiktorov, V. Gruzinskis, L. Reggiani, L. Varani, J. C. Vaissiere, "*Microscopic investigation of large-signal noise in semiconductor materials and devices*", Proceedings of SPIE 5113, 252 (2003).

[14] D. Persano Adorno, M.C. Capizzo, M. Zarcone, "*Wave-mixing effects on electronic noise in semiconductors*", J. Computat. Electron. 5, 475 (2006);

[15] D. Persano Adorno, M.C. Capizzo, M. Zarcone, "*Changes of Electronic Noise Induced by Oscillating Fields in Bulk GaAs Semiconductors*",Fluctuation and Noise Letters 8, L11 (2008).

[16] D. Persano Adorno, M. C. Capizzo and N. Pizzolato, "*Frequency Influence on the Hot-Electron Noise Reduction in GaAs Operating under Periodic Signals*", Acta Physica Polonica A 113, 979 (2008).

[17] Ghosh P. K., Sen M. K. and Bag B. C., "*Kinetics of self-induced aggregation of Brownian particles: Non-Markovian and non-Gaussian*

features", Phys. Rev. E, 78 (2008) 051103.

[18] Ghosh P., Chattopadhyay S. and Chaudhuri J. R., "*Enhancement of current commensurate with mutual noise–noise correlation in a symmetric periodic substrate: The benefits of noise and nonlinearity*",Chem. Phys., 402 (2012) 48.

[19] Nakada K.,Yakata S. and Kimura T., "*Noise-Induced Transition of Mutual Phase Synchronization in Coupled Spin Torque Nano Oscillators*", IEEE Trans. Magn., 48 (2012) 4558.

[20] Wang B., Sun Y. Q. and Tang X. D., *"Effects of non-Gaussian noise on a calcium oscillation system*", Chin. Phys. B, 22 (2013) 010501.

[21] Sen M. K.,S. Ray, A. Baura, B. C. Bag, "*Effect of multiplicative noise on the self-induced aggregation kinetics of Brownian particles*", Chem. Phys. Lett., 559 (2013) 117.

[22] J. M. G. Vilar, J. M. Rubi, "*Noise Suppression by Noise*", Phys. Rev. Lett. 86, 950 (2001).

[23] D. B. Walton, K. Visscher, "*Noise suppression and spectral decomposition for state-dependent noise in the presence of a stationary fluctuating input*", Phys. Rev. E 69, 051110 (2004).

[24] Y. Seol, K. Visscher, D. B. Walton, "*Suppression of Noise in a Noisy Optical Trap*", Phys. Rev. Lett. 93, 160602 (2004).

[25] R.N. Mantegna and B. Spagnolo, "*Noise Enhanced Stability in an Unstable System*", Nuovo Cimento D 17, 873 (1995).

[26] L. Gammaitoni, P. Hanggi, P. Jung, F. Marchesoni, "*Stochastic resonance*", Rev. Mod. Phys. 70, 223 (1998).

[27] B. Spagnolo, S. Spezia, L. Curcio, A. Fiasconaro, N. Pizzolato, D. Valenti, P. Lo Bue, E. Peri, S. Colazza, "*Noise effects in two different biological systems*"

Eur. Phys. J. B 65, 453 (2008).

[28] M.D. McDonnell and D. Abbott, "*What Is Stochastic Resonance? Definitions, Misconceptions, Debates, and Its Relevance to Biology*", PLoS Comput. Biol. 5, e1000348 (2009).

[29] Spagnolo, B., Dubkov, A. A., Pankratov, A. L., Pankratova, E. V., Fiasconaro, A. & Ochab-Marcinek, A., "*Lifetime of metastable states and suppression of noise in interdisciplinary physical models*," Acta Phys. Pol. 38, 1925 (2007)

[30] N. Pizzolato, A. Fiasconaro, D. Persano Adorno, B. Spagnolo, "*Resonant activation in polymer translocation: new insights into the escape dynamics of molecules driven by an oscillating field*", Phys. Biol. 7, 034001 (2010);

[31] N. Pizzolato, A. Fiasconaro, D. Persano Adorno, B. Spagnolo, *"Translocation dynamics of a short polymer driven by an oscillating force",* J. Chem.Phys. 138, 054902 (2013).

[32] N. V. Agudov, B. Spagnolo, "*Noise-enhanced stability of periodically driven metastable states*", Phys. Rev. E 64, 035102(R) (2001).

[33] A.A. Dubkov, N.V. Agudov, B. Spagnolo, "*Noise-enhanced stability in fluctuating metastable states*",Phys. Rev. E 69, 061103 (2004).

[34] D. Persano Adorno, N. Pizzolato, B. Spagnolo, "*External Noise Effects on the Electron Velocity Fluctuations in Semiconductors*", Acta Physica Polonica A 113, 985 (2008).

[35] D. Persano Adorno, N. Pizzolato, B. Spagnolo, "*The influence of noise on electron dynamics in semiconductors driven by a periodic electric field*", J. Stat. Mech. Theor. Exp., P01039 (2009).

[36] D. Persano Adorno, N. Pizzolato, D. Valenti, B. Spagnolo, "*External Noise Effects in Doped Semiconductors Operating Under sub-THz Signals*", Rep. Math. Phys. 70, 171 (2012).

[37] L. Varani, C. Palermo, C. De Vasconselos, J.F. Millithaler, J.C. Vaissi´ere, J.P. Nouger, E. Starikov, P. Shiktorov, V. Gruzinskis, *"Is It Possible To Suppress Noise By Noise In Semiconductors?*", Proc. Int. Conf. on Unsolved Problems of Noise and Fluctuations, Melville, New York, AIP Conf. Proc. 800, p. 474-479 (2005).

[38] U. Atxitia, O. Chubykalo-Fesenko, R.W. Chantrell, U. Nowak, A. Rebei, 'Ultrafast Spin Dynamics: "*The Effect of Colored Noise",* Phys. Rev. Lett. 102, 057203 (2009).

[39] T. Bose, S. Trimper, *"Correlation effects in the stochastic Landau-Lifshitz-Gilbert equation*", Phys. Rev. B 81, 104413 (2010).

[40] Glazov M. M., Sherman E. Ya. and Dugaev V. K., "*Two-dimensional electron gas with spin–orbit coupling disorder*", Physica E, 42 (2010) 2157.

[41] Glazov M. M. and Sherman E. Ya., "*Theory of Spin Noise in Nanowires*", Phys. Rev. Lett., 107 (2011) 156602.

[42] V.K. Dugaev, M. Inglot, E.Ya. Sherman, J. Barnas , "*Spin Hall effect and spin current generation in two-dimensional systems with random Rashba spin-orbit coupling*", Journal of Magnetism and Magnetic Materials, 324, (2012), 3573.

[43] Agnihotri P. and Bandyopadhyay S., "*Spin dynamics and spin noise in the presence of randomly varying spin-orbit interaction in a semiconductor quantum wire"***,** J. Phys.: Con- dens. Matter, 24 (2012) 215302.

[44] J. M. Kikkawa and D.D. Awschalom, "*Resonant spin amplicaton in n-type GaAs*", Phys. Rev. Lett. **80,** 4313-4316 (1998)

[45] J. Fabian, A. Matos-Abiague, C. Ertier, P. Stano and I. Zutic, "*Semiconductor Spintronics*", Acta Phys. Slov. **57,** 565-907 (2007)

[46] M.W. Wu, J.H. Jiang, M.Q. Weng, "*Spin dynamics in semiconductors*", Phys. Rep. **493,** 61-236 (2010)

[47] S.Spezia, D. Persano Adorno**,** N. Pizzolato and B. Spagnolo, "*Relaxation of electron spin during high-field transport in GaAs bulk*", J. Stat. Mech. Theor. Exp. P11033-13 (2010)

[48] S.Spezia, D. Persano Adorno**,** N. Pizzolato and B. Spagnolo, "*Temperature dependence of spin depolarization of drifting electrons in n-type GaAs bulks*", Acta Physica Polonica B **41** (5), 1172-1180 (2010).

[49] S. Spezia, D. Persano Adorno, N. Pizzolato, B. Spagnolo, *"New insight into electron spin dynamics in the presence of correlated noise*", J. Phys.: Condens. Matter. 24, 052204 (2012)

[50] S. Spezia, D. Persano Adorno, N. Pizzolato, B. Spagnolo, "*Effect of a fluctuating electric field on electron spin dephasing time in III-V semiconductors*", J.Phys.: Acta Physica Polonica B 43 (5) 1191 (2012).

[51] B.T. Jonker, G. Kioseoglou, A.T. Hanbicki, C.H. Li and P.E. Thompson, "*Electrical spin-injection into silicon from a feromagnetic metal/tunnel barrier contact*", Nature Phys. **3,** 542-546 (2007)

[52] I. Appelbaum, B. Q. Huang, and D. J. Monsma, "*Electronic measurement and control of spin transport in silicon*", Nature **447,** 295-298 (2007)

[53] S.P. Dash, S. Sharma, R.S. Patel, M.P. de Jong, R.Jansen, "*Electrical creation of spin polarization in silicon at room temperature*", Nature **462,** 491-494 (2009)

[54] Shiktorov P, Starikov E, Gruzinskis V, Reggiani L, Varani L and Vaissi´ere JC , "*MonteCarlo Calculation of Electronic Noise under High-Order Harmonic Generation*," Appl. Phys.Letters 80, 4759 (2002)

[55] González T, Pérez S, Starikov E, Shiktorov P, Gruzinskis V, Reggiani L, Varani L and Vaissiére JC, "*Microscopic investigation of large-signal noise in semuiconductor materials and devices, Noise in devices and circuits*", Proc. of SPIE 5113, 252 (2003)

[56] R.J. Elliott, "*Theory of the Effect of Spin-Orbit Coupling on Magnetic Resonance in Some Semiconductors*", Phys. Rev. 96, 266-279 (1954).

[57] Y. Yafet, "*g Factors and Spin-Lattice Relaxation of Conduction Electrons*" Solid State Physics, 14, edited by F. Seitz and D. Academic, Turnbull New York (1963).

[58] Donald A. Neamen, "*Semiconductor Physics and Devices: Basic Principles*", Third Edition Mc Graw Hill (2003)

[59] Safa Kasap, Peter Capper, "*Springer Handbook of Electronic and Photonic Materials*", Springer (2007)

[60] C. Kittel, "*Introduction to Solid State Physics*", 6th edn, Wiley, New York (1986)

[61] K. Seeger, " *Semiconductor Physics*", Springer (1982)

[62] H.M. van Driel, "*Optical effective mass of high density carriers in silicon*", Appl. Phys. Lett. 44, 617 (1984).

[63] E.O. Kane, "*Energy band structure in p-type Germanium and Silicon* ", J.Phys. Chem. Solids 1, 82 (1956).

[64] B. Lax, J.G. Mavroides, "*Statistics and Galvanomagnetic Effects in Germanium and Silicon with Warped Energy Surfaces*", Phys. Rev. 100, 1650 (1955).

[65] K. Tomizawa, "*Numerical Simulation of Submicron Semiconductor Devices*", Artech House Inc., Norwood, (1993).

[66] I. Knezevic, E.B. Ramayya, D. Vasileska, S. M. Goodnick, "D*iffusive Transport in Quasi-2D and Quasi-1D Electron Systems*", J. Comput. Theor. Nanosci. 6, 1725 (2009).

[67] M. Lundstrom, "*Fundamentals of carrier transport*", University Press, Cam- bridge, 2000.

[68] D.K. Ferry, C. Jacoboni, "*Quantum Transport in Semiconductor Devices*", Chapman and Hall, Cambridge, 1993.

[69] C. Jacoboni, P. Lugli, "*The Monte Carlo Method for Semiconductor Device Simulation*", edited by S. Selberherr, Springer, Wien, 1989

[70] C. Moglestue, "*Monte Carlo Simulation of Semiconductor Devices*", Chapman and Hall, London, 1993.

[71] D. Persano Adorno, M. Zarcone, G. Ferrante, "*Farinfrared harmonic generation in semiconductors: A Monte Carlo simulation*", Laser Phys. 10, 310-315 (2000)

[72] D. Persano Adorno, M. Zarcone, G. Ferrante, P. Shiktorov, E. Starikov, V. Gruˇzinskis, S. Pérez, T. Gonz´alez, L. Reggiani, L. Varani, J. C. Vaissi`ere, "*Monte Carlo simulation of high-order harmonics generation in bulk semiconductors and submicron structures*" Phys. Status Solidi C 1, 1367-1376 (2004).

[73] P.Y. Yu, M. Cardona, "*Fundamentals of Semiconductors*", Physics and Material Properties', Springer-Verlag, Berlin, 2003.

[74] C. Jacoboni, "*Theory of Electron Transport in Semiconductors*", Springer-Verlag, Berlin Heidelberg, 2010.

[75] D. Persano Adorno, M. Zarcone, G. Ferrante, "*High-Order Harmonic Generation Efficiency in n-Type Silicon and InP.*", Laser Physics 11, (2), 291 (2001).

[76] Martin Martinez, M.J., 1996, *Thesis,* Salamanca University.

[77] A. van der Ziel, "*Noise in Solid State Devices and Circuits*", NY: Wiley (1986).

[78] A. Papoulis, "*Probability, Random Variables, and Stochastic Processes",* New York: McGrawHill,3ed. (1991).

[79] *V.* Mitin, L.Reggiani, L. Varani*, "Noise alld Fluctuations Control* in *Electronic Devices",* Edited by A. BaJandin (2002).

[80] M. Sandén, O. Marinov, M. Deen, and M. Ostling, "*A new model for the low frequency noise and the noise level variation in polysilicon emitter BJTs*," IEEE Transactions on Electron Devices*,* 49, 514 (2002).

[81] G. Massobrio and P. Antognetti, "*Semiconductor Device Modeling with SPICE",* NY: McGraw-Hill, 2ed. (1993)

[82] F. N. Hooge, "*1/ f noise sources*," IEEE Transactions on Electron Devices, 41, 1926 (1994).

[83] C.W. Gardiner, *"Handbook of stochastic methods for physics, chemistry and the natural sciences*", Springer-Verlag, Berlin (1993).

[84] Askari G, Ghasemi K, Sadeghi HM, "*Microwave and Millimeter Wave Tech- nologies Modern UWB antennas and equipment*", edited by I Minin, Rijeka, In-Tech (2010).

[85] D. Barik, P. K. Ghosh, D. S. Ray, "*Langevin dynamics with dichotomous noise; direct simulation and applications*", J. Stat. Mech.: Theory Exp. P03010 (2006).

[86] T. Ando, A. B. Fowler, F. Stern, "*Electronic properties of two-dimensional systems*", Rev. Mod. Phys. 54, 437 (1982).

[87] W. Walukiewicz,H. E. Ruda, J. Lagowski and H. C. Gatos, "*Electron mobility in modulation-doped heterostructures*", Phys. Rev. B 30, 4571 (1984).

[88] M.A. Lodato, D. Persano Adorno, N. Pizzolato, S. Spezia & B. Spagnolo, "*External Noise Effects in Silicon MOS Inversion Layer*", Acta Physica Polonica B, 44(5), 1163 (2013).

[89] D. Persano Adorno, M.A. Lodato, N. Pizzolato, and B. Spagnolo, "*Hot-Electron Noise Features in Silicon Crystals Operating under Periodic Signals*", Lithuanian Journal of Physics, **54** (1), 20 (2014)

[90] Bena I., "*Dichotomous Markov Noise: Exact results for out-of-equilibrium systems*", Int. J. Mod. Phys. B, 20 (2006) 2825.

[91] J. Fabian, S. Das Sarma, *"Spin relaxation of conduction electrons"*, J. Vac. Sci. Technol. B 17, 1708-1715 (1999).

[92] S.A. Wolf, D.D. Awschalom, R.A. Buhrman, J.M. Daughton, S. von Moln´ar, M.L. Roukes, A.Y. Chtchelkanova, D.M. Treger, "*Spintronics: A Spin-Based Electronics Vision for the Future*", Science 294, 1488-1495 (2001).

[93] I. **Žutić**, J. Fabian, S. Das Sarma, "*Spintronics: Fundamentals and Applications*" Rev. Mod. Phys. 76, 323-410 (2004).

[94] D.D. Awschalom, M.E. Flatté, "*Challenges for semiconductor spintronics*" Nature Phys. 3, 153-159 (2007).

[95] M.E. Flatté, "*Silicon spintronics warms up*" Nature 462, 419-420 (2009).

[96] J. Fabian and S. Das Sarma, "*Spin Relaxation of Conduction Electrons in Polyvalent Metals: Theory and a Realistic Calculation",* Phys. Rev. Lett. **81,** 5624 (1998);

[97] J. Fabian and S. Das Sarma, "*Phonon-induced spin relaxation of conduction electrons in aluminum*", *Physical Review Letters* **83**, 1211 (1999).

[98] P. Li and H. Dery, "*Spin-Orbit Symmetries of Conduction Electrons in Silicon*" Phys. Rev. Lett. **107,** 107203-5 (2011);

[99] Y. Song and H. Dery, "*Analysis of phonon-induced spin relaxation processes in silicon*", Phys. Rev. B **86,** 085201-28 (2012)

[100] J.L. Cheng, M.W. Wu and J. Fabian, "*Theory of the Spin Relaxation of Conduction Electrons in Silicon*" Phys. Rev.Lett.104, 016601-4 (*2010)*

[101] O. D. Restrepo and W. Windl, "*Full First-Principles Theory of Spin Relaxation in Group-IV Materials*", Phys. Rev. Lett. **109,** 166604-5 (2012)

[102] J.M. Tang, B.T. Collins and M.E. Flatté, "*Electron spin-phonon*

interaction symmetries and tunable spin relaxation in silicon and germanium"Phys. Rev. B **85,** 045202-7 (2012)

[103] A.W Overhauser, "*Paramagnetic relaxation in metals*", Phys. Review 89, 689-700 (1953)

[104] D. Persano Adorno, C. Graceffa, N. Pizzolato and M.A., Lodato "*Monte Carlo simulation of spin relaxation of conduction electron in silicon*", Lithuanian Journal of Physics, **54** (1), 25 (2014)

Appendix A

A.1 List of Pubblications

1. M.A. Lodato, D. Persano Adorno, S. Spezia, N. Pizzolato, B. Spagnolo *"External Noise Effects in Silicon MOS Inversion Layer",* Acta Physica Polonica B, 44 (5), 1163 (2013).

2. M.A. Lodato, D. Persano Adorno and B. Spagnolo, "Hot-electron noise features in Silicon Crystals operating under periodic signals", Lithuanian Journal of Physics, 54 (1), 20 (2014)

3. D. Persano Adorno, C. Graceffa, N. Pizzolato and M. A. Lodato "Monte Carlo simulation of spin relaxation of conduction electrons in Silicon" Lithuanian Journal of Physics, 54 (1), 25 (2014)

A.2 International conferences

1. Poster presentation: *External Noise Effects in Silicon MOS Inversion Layer,* D. Persano Adorno, M.A. Lodato, S. Spezia, N. Pizzolato, B. Spagnolo, in "25th Marian Smoluchowski Symposium on Statistical Physics" (Cracow, Poland, 9-13 settembre 2012).

2. Poster presentation: *Hot-electron noise features in Silicon Crystals operating under periodic signals*, M.A. Lodato, D. Persano Adorno and B.

Spagnolo, in "15th International Symposium on Ultrafast Phenomena in Semiconductors" (Vilnius, Lithuania 25-28 August, 2013*)*

3. Poster presentation: *Monte Carlo simulation of spin relaxation of conduction electrons in Silicon*, Persano Adorno, C. Graceffa, N. Pizzolato and M. A. Lodato, in "15th International Symposium on Ultrafast Phenomena in Semiconductors" (Vilnius, Lithuania 25-28 August, 2013*)*

4. Poster presentation: *Noise can enhance stability in Si bulk?,* M. A. Lodato, D. Persano Adorno, N. Pizzolato and B. Spagnolo, in "27th Marian Smoluchowski Symposium on Statistical Physics" (Zakopane, Poland, 22-26 settembre 2014).